Microglial Neuroinflammation-Independent Reversal of Demyelination of Corpus Callosum by Arsenic in a Cuprizone-Induced Demyelinating Mouse Model

Shaivya Kushwaha[1,2] · Joel Saji[3] · Rahul Verma[2,3] · Vikas Singh[1,4] · Jamal Ahmad Ansari[1,2,5] · Shubhendra Kumar Mishra[1,6] · Opalina Roy[1] · Satyakam Patnaik[2,3] · Debabrata Ghosh[1,2]

Abstract

Demyelination is the loss of myelin in CNS, resulting in damaged myelin sheath. Oxidative stress and neuroinflammation play a key role in inducing demyelinating diseases like MS; hence, controlling oxidative stress and neuroinflammation is important. Cuprizone (CPZ), a copper chelator, generates oxidative stress and neuroinflammation, thereby inducing demyelination. Therefore, the CPZ-induced demyelinating mouse model (CPZ model) is widely used in research. The present study was intended to unravel a mechanism of inhibition of demyelination by arsenic in a CPZ model, which is otherwise known for its toxicity. We investigated an alternative mechanism of inhibition of demyelination by arsenic through the reversal of SOD1 activity employing in silico analysis, analytical chemistry techniques, and in vitro and in vivo experiments. In vivo experiments showed protection of body weight, survivability, and myelination of the corpus callosum in CPZ and arsenic-co-exposed animals, where neuroinflammation was apparently not involved. In vitro experiments revealed that arsenic-mediated reversal of impaired SOD1 activity leads to reduced cellular ROS levels and better viability of primary oligodendrocytes. Reversal of SOD1 activity was also observed in the corpus callosum tissue isolated from experimental animals. In silico and analytical chemistry studies revealed that similar to copper, arsenic can potentially bind to CPZ and thereby make the copper freely available for SOD1 activity. Suitable neurobehavior tests further validated the protective effect of arsenic. Taken together, the present study revealed that arsenic protects oligodendrocytes and demyelination of corpus callosum by reversing CPZ-induced impaired SOD1 activity.

Keywords Demyelination · Microglia · Cuprizone · Arsenic · Neuroinflammation · Corpus callosum · SOD1

Abbreviations

CPZ/Cpz	Cuprizone
Cu/Zn SOD	Cu/Zn super oxide dismutase
CNS	Central nervous system
MS	Multiple sclerosis
ROS	Reactive oxygen species
RR-MS	Relapsing-remitting MS
PBS	Phosphate buffer saline
PDGF	Platelet-derived growth factor
FGF	Fibroblast growth factor
DCFH-DA	2′,7′-Dichlorofluorescein diacetate
PFA	Paraformaldehyde

Joel Saji and Rahul Verma contributed equally.

✉ Satyakam Patnaik
satyakampatnaik@iitr.res.in

✉ Debabrata Ghosh
debabrata.ghosh@iitr.res.in; debabrataghosh78@gmail.com

1 Immunotoxicology Laboratory, System Toxicology Group, FEST Division, CSIR-Indian Institute of Toxicology Research (CSIR-IITR), Vishvigyan Bhawan, 31, Mahatma Gandhi Marg, Lucknow, Uttar Pradesh 226001, India

2 Academy of Scientific and Innovative Research (AcSIR), Ghaziabad 201002, India

3 Water Analysis Laboratory, Drug and Chemical Toxicology Group, FEST Division, CSIR-Indian Institute of Toxicology Research, Lucknow, Uttar Pradesh 226001, India

4 Department of Neurosciences, Lerner Research Institute, Cleveland Clinic, Cleveland, OH 44195, USA

5 Genome Instability and Chromatin Remodeling Section, NIH-National Institute of Aging, Baltimore, USA

6 Department of Pediatrics, Division of Neonatology, McGill University Health Centre-Research Institute (RI-MUHC), Montreal, QC, Canada

HBSS	Hanks Balanced Salt Solution
FBS	Fetal bovine serum
DAPI	4′,6-Diamidino-2-phenylindole
MBP	Myelin basic protein
IAEC	Institutional Animal Ethics Committee
RO water	Reverse osmosis water
BSA	Bovine serum albumin
NAC	N acetyl cysteine
RT	Room temperature
MFI	Mean fluorescence intensity
TEM	Transmission electron microscopy
DMSO	Dimethyl sulfoxide
DFT	Density functional theory
ANOVA	One-way analysis of variance
SEM	Standard error mean
IL-6	Interleukin 6
TNF-α	Tumor necrosis factor alpha
m/z	Mass to charge ratio
AFS	Atomic force spectrophotometry
ICP-MS	Inductively coupled plasma mass spectrometry
FTIR	Fourier-transformed infrared spectroscopy
ITC	Isothermal titration calorimetry
bd wt	Body weight

Introduction

Demyelination is the loss of myelin sheath insulation of the nerve axons, which leads to diseases like multiple sclerosis (MS) with impaired neuronal response [1]. Immune dysregulation arising from the complex interaction between genetic predisposition and environmental factors causes demyelinating disease. Among genetic and environmental factors, oxidative stress and inflammation play a central role in the etiology, progression, and clinical symptoms of demyelinating disease [2]. Continuous exposure to reactive oxygen species (ROS) like hydroxyl radical (OH•) and superoxide radical (O-•) from exogenous and endogenous sources may lead to oxidative stress. Oxidative stress can damage cellular components like lipids, proteins, and nucleic acids, leading to cellular death, which in turn contributes to the pathophysiology of the demyelinating disease in the CNS [2–4]. Oxidative stress is controlled naturally by enzymatic and non-enzymatic antioxidant defense systems. Cu/Zn superoxide dismutase (SOD1) is the first line of defense and the key enzyme in controlling oxidative stress, thereby protecting oxygen-free radical-mediated damage of biomolecules [5]. SOD1 reduces the cellular superoxide anion to H_2O_2 where copper (Cu) plays an indispensable role in the catalytic site of the enzyme, and zinc (Zn) is involved in proper protein folding and stability. H_2O_2 is further

reduced to H_2O, where catalase plays a prominent role along with other enzymes like glutathione peroxidase (GPx) and peroxiredoxin (Prx) [6]. H_2O_2 can be converted to a more reactive hydroxyl radical (•OH) in the presence of metal ions. Hydroxy radicals can damage the cells more severely by reducing the disulfide bond than any other free radicals [7]. Therefore, SOD1 and catalase both should act simultaneously to neutralize oxidative stress. Cuprizone, a copper chelator, can degenerate oligodendrocytes and induce demyelination when given to animals with regular chow diet [4, 8, 9]. Induction of synchronous and anatomically reproducible demyelination made the CPZ model widely used to study demyelinating diseases like MS [10, 11]. The cuprizone model can be used to study the multifaceted interaction of oxidative stress, neuroinflammation, and oligodendrocyte degeneration [4, 9, 11]. CPZ induces oligodendrocyte death and demyelination either by intrinsic pathway, where cellular oxidative stress plays the main role or by extrinsic pathway, where the local immune cell-mediated inflammatory environment potentially initiates or aggravates the demyelination [12]. It has been observed that the oligodendrocyte perikaryon is initially affected by CPZ as revealed by the early downregulation of myelin-specific gene and extensive death of oligodendrocytes prior to demyelination in the corpus callosum [13, 14]. Interestingly, oligodendrocytes are specifically susceptible to CPZ intoxication owing to their high metabolic demand for the synthesis of myelin [10]. CPZ binds and stabilizes the copper ions [15, 16], which can potentially induce oxidative stress by affecting the function of the antioxidant system, such as SOD1. Coincidentally, a decreased level of copper was detected in the brains of Swiss mice treated with CPZ for 3–4 weeks [17], and reduced SOD1 activity was observed in MS patients [18]. CPZ-induced demyelination of the corpus callosum and other white matter regions of the brain coincides with various neurobehavioral changes like sickness, catalepsy, gait abnormality, hind limb paralysis, increased climbing behavior, impaired motor coordination, cognitive function and spatial memory, social behavior, and anxiety [5, 8, 11].

The present study comprehensively sought to identify the mechanism of inhibition of demyelination by arsenic in a CPZ model focusing on the corpus callosum. In silico analysis, analytical chemistry techniques, and in vitro and in vivo experiments were employed for the study. We checked the body weight, survivability, and the level of myelination in the corpus callosum. We have also checked the level of microglial inflammation. In vitro studies with primary oligodendrocytes were also performed to check the role of SOD1 activity in the protection of demyelination by arsenic. In silico analyses were performed to check the interaction of arsenic with SOD1. Analytical

chemistry methods like ICP-MS, FTIR, AFS, and ITC were used to establish the binding of arsenic and copper with cuprizone. The study was further extended to validate the impact of protection of corpus callosum demyelination through neurobehavioral tests like tail suspension test and grip strength test. Overall, the study revealed an interesting alternative mechanism of protection from demyelination by an infamous environmental toxicant, arsenic.

Experimental Procedure

Reagents and Antibodies

Sodium arsenite (NaAsO$_2$), phosphate-buffered saline (PBS), Papain, percoll, platelet-derived growth factor (PDGF), fibroblast growth factor, T3 Stock, NAC supplement, NAC supplement, poly-L-lysine solution, Triton X-100, Tween-20, paraformaldehyde (PFA), chloroform, acetone, 2′,7′-dichlorofluorescein diacetate (DCFH-DA), minocycline hydrochloride, Black-gold II myelin staining kit (AG105) were procured from Sigma-Aldrich. Hanks Balanced Salt Solution (HBSS), glycerol and methanol (LC grade) were procured from Merck-Millipore. Cell culture medium (DMEM/F12), fetal bovine serum (FBS), neurobasal medium, B27 supplement, penicillin–streptomycin, N-2 supplement, 4′,6-diamidino-2-phenylindole (DAPI), procartaplex for IL-6/TNF-α, trypsin–EDTA, and SOD activity kit (EIASODC) were procured from Thermo-Fisher Scientific. Vectashield mounting medium was procured from Vectorlabs, and bovine serum albumin was indented from Amresco. Antibody for Iba1 was procured from Millipore (MABN92), antibody for myelin basic protein (MBP) was procured from Abcam (Ab40390), and goat anti-mouse secondary antibody (AlexaFluor 594, A-21145) and goat anti-rabbit secondary antibody (FITC, F2765) were procured from Thermo Scientific.

Animal Husbandry and Treatment

Six- to 8-week-old male BALB/c mice were procured from the animal house facility of the CSIR-Indian Institute of Toxicology Research (CSIR-IITR). All the protocols of the study were approved by the Institutional Animal Ethics Committee (IAEC) of the CSIR-IITR in Lucknow, India (IITR/IAEC/73/17). All experiments were conducted in accordance with the standards established by the CPCSEA of the Ministry of Environment and Forests, Government of India, New Delhi, India. Mice were housed at 25 ± 3 °C, 12/12 h light/dark cycle with rodent chow diet (Cat. no: 1324, Altromin, Germany), and RO water (Reverse Osmosis water) supplied ad libitum. An investigator who was unaware of the treatment groups randomly separated the animals into four groups (10 animals in each group): control, cuprizone (0.2% in diet), arsenic (0.38 mg/kg bd wt.), cuprizone + arsenic. The treated animals were gavage fed daily with 0.38 mg/kg bd wt. sodium arsenite for 30 days, and the control group received only RO water. Arsenic dose selection was based on our previous studies [19–21]. Animals were also exposed to cuprizone mixed with rodent chow diet (0.2% w/w). Following a 30-day treatment regimen, animals were sacrificed and used for various analyses. In another experiment, animals were divided into three groups: control, cuprizone (0.2% w/w in food), and cuprizone + minocycline (33 mg/kg bd wt.). Animals were exposed to cuprizone through diet (0.2% w/w in food) for 30 days. Minocycline (33 mg/kg bd. wt.) was administered intraperitoneally every other day for the last 2 weeks before the mice were sacrificed. Each time, a fresh stock of minocycline was prepared by dissolving in water and filter-sterilizing it. The weights of mice were checked weekly in order to study the changes in body weight. Following scheduled exposure, animals were sacrificed. Primary microglia were isolated (ex vivo microglia) and used to measure cytokines, whereas the whole brain was isolated and used for immunohistochemistry and Black gold myelin sheath staining. The corpus callosum from brain was isolated, and its lysate was prepared and used for measuring superoxide dismutase (SOD) activity. Control and treated animals were also subjected to tail suspension and grip strength tests.

Isolation of Primary Microglia

Primary microglia were isolated from adult animals (ex vivo *microglia*) using the protocol published from our laboratory [21]. Briefly, animals were deeply anesthetized and perfused with 4% paraformaldehyde. Brains were separated from experimental animals, chopped and enzymatically digested with Papain (20 U/ml) at 37 °C for 20 min. The digested tissue was triturated with a 1-ml micropipette to make the tissue homogenate. The homogenate was mixed with 30% isotonic percoll and centrifuged at $500 \times g$ for 20 min at 20 °C. Microglia were collected from the pellet and washed with culture medium. Isolated microglia (5×10^4 cells/100 μl/ well) were cultured in DMEM/F12, supplemented with 2% FBS and N-2 supplement for 18 h. Post 18-h incubation, the culture medium was collected and assayed for cytokines.

Primary Oligodendrocyte Culture and Treatment

Primary oligodendrocytes were differentiated from embryonic brain cells following a published protocol [22] and used for in vitro experiments. In brief, mouse embryos were separated from the uterus of 15–17-day pregnant mice. Brains of four to five embryos were isolated; cortices were aseptically removed and put in 7-ml chilled Hanks' balanced salt solution (HBSS) buffer, followed by meninges removal. The meninges-free cortices were placed into 3 ml of neurobasal medium and triturated for 1 min using 1-ml pipette tip, followed by addition of 0.8 ml of trypsin (0.25%) and kept for 15 min at 37 °C, vortexing every 2 min for 30 s. Fetal bovine serum (0.8 ml FBS) was added to the brain homogenate to neutralize the effect of trypsin, filtered through 40-µm nylon mesh and centrifuged at 1000 rpm for 5 min at 4 °C. The cell pellet was resuspended in 4-ml oligosphere growth medium (neurobasal growth medium, 0.5 mM L-glutamine, 10 ng/ml PDGF, 20 ng/ml FGF, 2% Pen-Strep antibiotic solution, $1 \times N2$, $1 \times B27$, 0.1 µM D-Biotin, 0.1% BSA solution) and incubated in a CO_2 incubator for 3–5 days depending on the formation of oligosphere. The oligospheres were dissociated into a single-cell suspension by pipetting with a 1-ml microtip. Cells were centrifuged (1000 rpm for 5 min at 20 °C) and resuspended (5000 cells/200 µl/well in 96-well plate) in oligosphere growth media and seeded in the poly-D-lysine–coated 96-well plate. After 3–4 days, the oligosphere growth media was replaced with oligodendrocyte differentiation medium (neurobasal medium, 0.5 mM L-glutamine, 2% penicillin streptomycin antibiotic solution, $1 \times N2$, $1 \times B27$, 0.1 µM D-Biotin, 0.1% BSA solution 0.1 mg/ml NAC, 15 nM triiodothyronine) and continued for 8 days or till the mature oligodendrocytes were observed. Mature oligodendrocytes were used for various in vitro experiments.

Cryosectioning and Immunohistochemistry

Experimental animals were deeply anesthetized using ketamine and xylazine (60 and 20 mg/kg bd wt.) and perfused with 0.1 M PBS followed by 4% PFA in 0.1 M PBS through the left cardiac ventricle. The brains were dissected out and fixed overnight in 4% PFA. PFA-fixed brains were then transferred to sucrose gradients (15% and 30% in 0.1 M PBS) and left in each gradient for at least 24 h. Brains were rinsed thoroughly with 0.1 M PBS before each transfer. Brains were frozen to −20 °C in tissue freezing medium for 5–6 h, and 20-µm coronal sections were cut in a cryo-microtome (Microm HM 520, Labcon, Germany) from the similar brain region (0.5 anterio posterior to −1.5 anterio posterior relative to bregma). Sections were collected in 0.1 M PBS, washed for 15 min in the same solution to remove the freezing medium, and stored at 4 °C if not used immediately. Cryosections were washed with 0.1% PBST (0.1% Triton X-100 in $1 \times PBS$) and subjected to epitope retrieval by microwaving the sections in 0.01 M citrate buffer until boiling. The traces of citrate buffer were removed from the sections by washing them with 0.1% PBST. Sections were permeabilized by treatment with 1% PBST for 30 min and then blocked with 10% horse serum for 1 h at RT. The sections were probed with the desired primary antibody and kept at 4 °C for 48 h. Following 48-h incubation with primary antibody, sections were re-probed with appropriate fluorescently labeled secondary antibody and washed with 0.1 M PBS. Nuclei were stained with DAPI, mounted with an antifade mounting medium, and observed under the Nikon Eclipse fluorescence microscope (Nikon Instrument Inc., Japan). The quantification of target protein-associated fluorescence was done using ImageJ software (https://imagej.nih.gov/ij/). Fluorescent images were transformed to 8-bit grayscale images, and the particle tool in ImageJ was used for the quantification of the percentage area occupied by target protein associated with fluorescence intensity and DAPI fluorescence for each image. For quantitative analysis of MBP-associated fluorescence, only the corpus callosum region was considered. Data were then reported as the percentage of target protein fluorescence and DAPI fluorescence in each unit of area [20].

Black-Gold II Myelin Sheath Staining

Coronal cryosections of brain were also stained with black-gold II myelin staining kit following the manufacturer's protocol to examine the extent of demyelination in the corpus callosum. Black-gold II (0.3% in 0.9% NaCl) and 1% sodium thiosulfate solution were pre-heated at 60 ˚C. Cryosections were rehydrated in MilliQ water for 2 min, followed by the incubation of the slide in black gold II solution at 60 °C for 12 min. During the incubation, slides should be monitored for the color change of myelin fiber from dark red to black. The sections were rinsed with Milli-Q water twice for 2 min and incubated with 1% sodium thiosulfate for 3 min at 60 °C, followed by washing with Milli-Q water three times for 2 min each. Finally, slides were dehydrated using graded alcohol for 5 min in each grade, incubated in xylene for 2 min, mounted with DPX on glass slides, and observed under a bright field microscope (Leica Dmi1). Quantitative analysis of the severity of demyelination (corpus callosum) was measured from the Black gold myelin sheath stain-stained brain section through a double-blind fashion, and the severity of demyelination was rated on a three-point scale of 1, 2, and 3 in which a lower (defined as 1), moderate (defined as 2), and higher (defined as 3) score shows a lesser, medium, and greater pathology, respectively.

Detection of Cytokine Levels in Ex Vivo Microglia Culture Supernatant

Ex vivo microglia were isolated from adult animals (ex vivo *microglia*) using the protocol published by our laboratory [21]. Isolated cells were cultured in 96-well culture plates (5×10^4 cells/100 µl/well for 18 h in DMEM/F12 medium supplemented with 2% FBS, 1% pen-Strep and N2 supplement, in a CO_2 incubator that maintained 37 °C, 5% CO_2, and 95% humidity. After 18 h, the cell culture supernatant was collected for cytokine detection. The level of cytokine in the microglia culture supernatant was measured using the Procarteplex mouse cytokine detection kit following the manufacturer's protocol. Briefly, 25 µl of magnetic bead-tagged target antibody was added to each well of the magnetic assay plate. The liquid was removed, and the plate was washed $3 \times$ with wash buffer using a hand-held magnet. Then, 50 µl of culture supernatant and standards was added to the magnetic beads coated plate and shaken (500 rpm) at room temperature for 120 min. Thereafter, 25 µl of biotinylated detection antibody was added and shaken for another 30 min, followed by the addition of 50 µl of streptavidin-PE to each well of the plate. Finally, the plate was washed $3 \times$ with wash buffer, and beads were resuspended in 150 µl of reading buffer and run on the Bio-Plex MAGPIX multiplex reader. The infrared (IR) fluorescence associated with various antibody-coated magnetic beads was measured to calculate the level of cytokines. The data were presented as a fold change of mean fluorescence intensity (MFI) over the control.

Transmission Electron Microscopy

The ultra-cellular myelin sheath structure of the corpus callosum was assessed through transmission electron microscopy (TEM). The corpus callosum was isolated from the brain of 4% PFA-perfused animals and sliced into small fragments of 2–3 mm. Glutaraldehyde (2.5%) was used to fix the parts overnight at 4 °C followed by post-fixation in osmium tetroxide (OsO4) for 2 h at room temperature. The pieces were first dried in an acetone gradient (10–100%), after which they were dehydrated in propylene oxide. After dehydration, the fragments were embedded in araldite and dodecyl succinic anhydride and baked for 2 days at 65 °C. The tissue blocks were prepared and sliced into 50–70-nm ultrathin slices using an ultramicrotome (Leica EM UC7). These slices were stained with lead citrate and uranyl acetate and studied under a transmission electron microscope (FEI, Technai G2 Spirit TWIN, USA). The images were taken from a sufficient number of areas at $15,000 \times$ and were evaluated from two animals in each group. The myelinated fibers in each area were manually counted and represented in scatter plot histograms [23].

Preparation of the Cuprizone Solution

The cuprizone solution was prepared freshly by dissolving cuprizone powder (C9012, Sigma-Aldrich) in 50% ethanol in ddH$_2$O. For proper dissolution of cuprizone, the solution was heated at 60 °C while being stirred for 15–20 min until all of the cuprizone was dissolved completely and filtered (0.2 µm). Each batch was used within 24 h. A stock solution of 10 mM was prepared, and the working solutions were prepared by diluting the stock solution in the cell culture medium as required.

Determination of Cell Viability

The impact of arsenic and cuprizone exposure on the viability of primary oligodendrocytes was assessed using MTT assay. Briefly, oligodendrocyte progenitor cells were seeded in 96-well culture plate at a density of 5000 cells/200 µl/well and kept in an oligodendrocyte differentiation medium for 8 days. On the 9th day, cells were treated with cuprizone (400 µM), sodium arsenite (500 nM), and $CuSO_4$ (0.5 µM) alone or in combination for 24 h. MTT (0.5 mg/ml) was added in each well of 96-well culture plate 2 h before the completion of incubation period and kept at 37 °C in a CO_2 incubator to allow the formazan crystal formation. The formazan crystals were dissolved in 100 µl of DMSO (Dimethyl sulfoxide), and the absorbance was recorded at 570 nm in a microplate reader (Ω fluostar, BMG labtech). Absorbance values were expressed as percent viability in a histogram.

SOD1 Activity Assay

The Cu/Zn SOD (SOD1) activity in corpus callosum tissue and primary mature oligodendrocyte lysate was measured using a SOD activity Kit (EIASODC, Thermo Fisher) following the manufacturer's protocol. Briefly, for measuring the SOD activity in tissue lysate, as the treatment in experimental animals was completed, the animals were deeply anesthetized using ketamine and xylazine (60 and 20 mg/kg body weight, respectively), and their corpus callosum was isolated from the brain and immediately frozen it through liquid nitrogen. The tissue was washed through ice-cold PBS and homogenized in chilled PBS (100 mg tissue/700 µl PBS). The homogenized tissue was subsequently centrifuged at $1500 \times g$ for 10 min at 4 °C, and the supernatant was collected for cytosolic SOD measurement. The homogenized tissue lysate was diluted at a 1:4 ratio in assay buffer. Each well of a 96-well assay plate received 10 µl of the diluted sample, 50 µl of $1 \times$ substrate, and 25 µl of $1 \times$ xanthine oxidase. After 20 min of incubation, the plate was read at 450 nm. For determining the SOD activity in mature oligodendrocytes, the oligodendrocyte progenitor cells

were seeded in 6-well culture plate at a density of 1×10^5 cells/2 ml/well and kept in oligodendrocyte differentiation medium for 8 days. On the 9th day, the mature oligodendrocytes were pre-treated with sodium arsenite (500 nM) and $CuSO_4$ (0.5 µM) for 24 h, followed by cuprizone (400 µM) treatment for 20 min. Following treatment, cells in the culture dish were washed with PBS and then harvested through trypsinization. The cells were then transferred into the tube on ice and centrifuged two times at $250 \times g$ for 10 min at 4 °C. Each time, the supernatant was discarded, and the cell pellet was suspended in ice-cold PBS (100 mg of cell pellet/700 µl PBS). The cell homogenate was then centrifuged at $1500 \times g$ for 10 min at 4 °C, and the supernatant was collected to measure the cytosolic SOD1 activity. The cell lysate was diluted at a 1:4 ratio in assay buffer. Each well of a 96-well assay plate received 10 µl of diluted sample, 50 µl of $1 \times$ substrate, and 25 µl of $1 \times$ xanthine oxidase. After 20 min of incubation, the plate was read at 450 nm. The SOD1 activity was calculated from a standard curve of SOD1 standards, which were provided with the kit, and the data was represented as unit/ml where one unit of SOD1 is the amount of enzyme causing half the maximum inhibition of 1.5 mM nitro blue tetrazolium reduction in the presence of riboflavin at pH 7.8 and 25 °C.

Measurement of Cellular ROS

To determine the ROS generation, oligodendrocyte progenitor cells were seeded in 96-well plate (5000 cells/200 µl/well) and kept in oligodendrocyte differentiation medium for 8 days. On the 9th day, cells were treated with sodium arsenite (500 nM) and $CuSO_4$ (0.5 µM) for 24 h. The following day media was changed, and cells were treated with 100 µM DCFDA for 20 min, followed by 30-min incubation with cuprizone (400 µM). DCFDA fluorescence intensity was recorded at excitation 485 nm and emission 420 nm in a microplate reader (Ω fluostar, BMG labtech). Fluorescence intensity was expressed as fold change to control and represented in violin plot with individual data points.

Tail Suspension Test

A tail suspension test was performed in experimental animals on completion of the treatment regimen following a published protocol [24]. The animals were suspended upside down by their tails in the tail suspension box, 55 cm above the table's surface. The experiment lasted 7 min, and the camera system recorded the immobility of mice for 6 min. The immobility time was considered only when mice hung passively and completely motionless. The recorded immobilization time was represented in a hybrid scatter-bar graph.

Grip Strength Test

Grip strength test was performed for the experimental animal following a published protocol [25] using a grip strength meter (TSE, Germany v.2.32). Animals ($n = 13$) were exposed to arsenic (0.38 mg/kg bd. wt.) and cuprizone (0.2% in chow diet) alone or in combination for 30 days and subjected to grip strength test. The forelimbs were placed on the tension bar, and the mice were pulled back gently until they released the bar. The maximal grip strength (pounds) value of the mouse that is displayed on the screen was recorded, and the process was repeated $3 \times$ for each of the animals.

Histopathology

On completion of the experimental regimen, animals were perfused with PBS, and the liver, kidney, and heart were isolated and fixed in 4% paraformaldehyde for 48 h at room temperature. Paraformaldehyde-fixed tissues were cut into small pieces, dehydrated through a series of graded alcohols, embedded in paraffin, and tissue blocks were prepared. Using a regular microtome, 5-µm-thick sections were cut. Sections were stained with hematoxylin and eosin, followed by visualization under a bright field microscope (Leica Dmi1).

Preparation of CPZ:M Complexes

Initially, 2 mM stock solutions of the three reagents, cuprizone (CPZ) (in methanol), $CuSO_4 \cdot 5H_2O$, and $NaAsO_2$ (in Milli Q) were prepared. CPZ was analyzed using direct injection ESI–MS. Samples for the CuCPZ and AsCPZ complexes were prepared by mixing aqueous solutions of $CuSO_4 \cdot 5H_2O$ and $NaAsO_2$ with CPZ solution in a stoichiometric ratio of 1:3 (v/v) respectively, and gradually raising the pH to ~ 8 by adding small aliquots of 1 M NaOH. The two reactions with the molar ratio of 1:3 (Metal ion:CPZ) were allowed for 60 min, after which these reactions were quenched by adding excess methanol. In the case of CuCPZ, the progressive appearance of blue color confirmed the complexation reaction, which was further diluted with methanol to obtain a final concentration of 100 µM [26]. Similarly, an AsCPZ complexation reaction was carried out. For Cu/AsCPZ complexation reaction, a similar approach was chosen with the exception that a 1:2 molar ratio was opted, and after the appearance of a pale blue color, post 60 min, the reaction was diluted in methanol to obtain a final concentration of 100 µM. The samples obtained were subjected to various spectroscopic investigations.

FTIR

FTIR spectra were recorded on a Nicolet iS-5 FT-IR spectrometer with a single beam in the range 500–4000 cm^{-1} using an ATR module.

Mass Spectrometry to Analyze CPZ:M Complexes

Prior to precipitate formation, during the early course of the CPZ:M complexation reaction, samples are aliquoted, filtered through a 0.2-mm syringe filter, and subjected to mass analysis. The samples were analyzed by direct injection with the 5600^{+} Triple TOF Mass Spectrometer (SCIEX, Framingham, MA, USA) in positive mode at a 10 µL/min flow rate. The nebulizer gas and heater gas were set at 18 psi, and the curtain gas was set at 20 psi. The ion spray voltage was set to + 5000 V with a declustering potential of + 100 V. The TOF scan was performed over the 50–1000 Da mass range [27].

ICP-MS to Analyze CPZ:M Complexes

Initially, three different stock solutions (2 mM, 5 mM & 10 mM) of CPZ (in methanol), $CuSO_4 \cdot 5H_2O$, and $NaAsO_2$ (in Milli Q) were prepared. As discussed in the above section, all three complexation reactions (CuCPZ, AsCPZ, and Cu/AsCPZ) at the above three concentrations were allowed overnight, followed by centrifugation at 10,000 rpm for 10 min to precipitate out the complexed product from the solution, digested with HNO_3, and analyzed by ICP-MS (Thermo Scientific iCAP™ RQ ICP-MS in KED mode) subsequently. Before the analysis, a calibration curve in the range of 50 ppt to 100 ppb was plotted using NIST-certified reference standards of Cu and As. The above three concentrations were chosen to identify all the possible metal–ligand interactions in the mass spectrum quantitatively. Milli Q blanks were also analyzed alongside the samples to check the presence of leftover samples for any cross-contamination. All samples were run in batches including blanks and standards and studied in duplication. Qtegra software was utilized for data integration and processing.

ITC to Assess the Competitive Binding Potential of As with CPZ in the Presence of Cu

Isothermal titration calorimetry (ITC) experiments were performed using a MicroCal ITC$_{200}$ (MicroCal Inc., Northampton, MA) instrument. All binding experiments were performed at 37 °C. Before the actual experiment, a series of ITC experiments were performed to optimize the metal–ligand concentrations and injection parameters to increase optimal bonding interactions with the target binding sites, which are as follows: initial delay, 8 s; injection volume, 2 µl; injection duration, 4 s; spacing, 180 s; filter period, 5 s. In a typical experiment, aliquots (2 µL) of aqueous metal solution (Cu/As, 3 mM) were sequentially injected (~ 25 injections) from a rotating syringe (syringe rotation = 750 rpm) into a stirred sample of 500 µM CPZ solution. This dilution leads to disaggregation, resulting in the isothermal absorption of heat from surroundings. The equilibrium constant (K), the binding stoichiometry (n), and the molar enthalpy (ΔH°) were obtained from the titration curve. All the solutions were degassed before titrations were performed. Each of the individual experiments was performed twice to ascertain repeatability and precision. The isotherms were fitted with the Origin V7.0 software using the on-site fitting model, excluding the first injection.

Molecular Docking and Simulation

Hardware and Software

This study used a rack server with an Intel® Xenon® Gold 6130 2.80 GHz processor, 128 GB RAM, and a 32-core benchmark to run Windows 10. Open-source molecular modeling simulation software was used; AutoDock V4.2 by the Scripps Research Institute for predicting binding sites and modes, and Gaussian 16W, Gauss View, and Discovery Studio Visualizer were used alone or in combination for geometry optimization and preparation of macromolecules and ligand (MAH).

Dock Preparation of Protein and CPZ

Proteins and metal: minimum energies were optimized by Gaussian View 6.1 and Discovery Studio Visualizer 3.5, respectively. The minimization command reduces the significance of metal–ligand and protein-metal–ligand molecular models using Minimization Gaussian 16W and AutoDock V4.2 (molecular modeling toolkit) algorithms, respectively [28, 29]. Since the 3D structure of CPZ is unavailable in any database, its structure was created using Discovery Studio Visualizer [30]. Structure of superoxide dismutases (SOD) protein were built using crystal structure (Protein Data Bank; ID 1CB4), and energy optimization was done using AutoDock V4.2 software. The metal energy and coordination were optimized by Gaussian 16W [31, 32]. Cu^{2+} and As^{3+} cations effectively chelate with CPZ through the N 2-N 3 atom in the hydrazide group of the CPZ molecule. The complex structure was geometrically optimized using UFF (universal force field), which reproduces the most structural features across all periodic tables [33]. It is capable of optimizing geometry for all elements, and it works well with both inorganic and organometallic elements. Furthermore, the docking of metal–ligand starts with protein–ligand energy minimization using AutoDock V4.2 software, with

each grid map consisting of $126 \times 126 \times 126$ grid points. During each docking experiment, 10 runs were performed, and the population size was set at 150; the maximum number of evaluations was 2.5×10^5; the maximum number of generations was 27,000; the rate of gene mutation was 0.02, and the cross-over rate was 0.8. The default setting was used for the remaining parameters. The root means square deviation (RMSD) tolerance for each docking experiment was set at 2.0 Å. A torsional DOF (degree of freedom) of 0.2983 was set as the coefficient for every ligand molecule for docking, and the docking results were clustered to find the binding free energy and optimal docking energy conformation. The best-docked structure elucidating their binding to receptors was considered for further analysis. In the cluster analysis, a total of 10 conformations were used, and the similarity of docked structures was measured by computing the RMSD between the coordinates of the atoms. It was observed, families of similar clusters yielded comparable RMSD values into which they were grouped. The RMSD cluster analysis was performed using the ligand atoms. The docking experiments were carried out using structurally similar collections ranked in order of increasing energy at 298.15 K. All the conformations were clustered together and ranked by the lowest binding energy. The Discovery Studio visualization 3.5 system carried out the structure file visualization.

DFT Calculations

All calculations reported in this study were obtained with the Gaussian 16W program package supported by Gauss View 6.1. Density functional theory (DFT) calculations were conducted at the Becke three-parameter hybrid functionals with non-local correlation functionals of Lee–Yang–Parr (B3LYP) [34, 35]. Direct Inversion in the Iterative Subspace (DIIS) method, a convergent SCF procedure, was used to optimize the gas phase geometry of copper, arsenic, cuprizone, and cuprizone-complexes at three different binding sites (NN, NO, OO). LANL2DZ basis set was used in all calculations, along with the corresponding effective core potential (ECP), for copper metal [34, 35]. For hydrogen (H) valence double zeta basis set, 6-31G, and for C, N, O, and Cl non-hydrogen atoms, valence double zeta plus diffuse and polarization functions, 6-31G (d,p) as the basis set was employed for the calculations [36]. Furthermore, the calculation of DFT energy profiling of transition states and intermediates of CuCPZ, AsCPZ, and Cu/AsCPZ complexes was performed with the above-optimized method using the CPCM model in MeOH [36].

Statistical Analysis

Data were presented as mean $\pm$ SD (standard deviation) or mean $\pm$ SEM (standard error of the mean). Statistical analysis was performed in GraphPad Prizm. Analysis of more than two groups was performed by one-way analysis of variance (ANOVA) followed by Tukey's post-test for comparing multiple groups or two-way ANOVA. A value of $p < 0.05$ was considered statistically significant.

Results

Arsenic Prevents Weight Loss and Increases Survivorship of Cuprizone-Exposed Balb/c Mice

Cuprizone exposure through chow diet (0.2% w/w) induces a progressive loss in body weight in experimental animals, leading to death. In the present study, cuprizone exposure induced severe body weight loss following 30 days of cuprizone exposure, whereas arsenic (0.38 mg/kg bd wt) co-exposure through oral gavage along with cuprizone significantly protected the loss of body weight. Arsenic exposure alone did not induce any significant alteration in body weight compared to control animals; a steady increase in body weight was observed (Fig. 1A). Simultaneously, the CPZ-induced death also followed a similar pattern. Arsenic-only exposure induced death of only one animal out of 11 animals during the entire exposure period, whereas CPZ induced death of seven animals out of a total of 13 animals. Only three animals died out of 11 animals in the CPZ-arsenic co-exposed group during the exposure period, showing a protective effect of arsenic on CPZ-induced death (Fig. 1B).

Arsenic Protects Cuprizone-Induced Demyelination of Corpus Callosum in Balb/c Mice

The cuprizone-induced demyelinating mouse model is commonly used to investigate the demyelination and remyelination-associated process. In the present study, we examined the effect of a low dose of arsenic co-exposed with cuprizone on the demyelination of corpus callosum in Balb/c mice. Animals were exposed to cuprizone through chow diet (0.2% w/w) and exposed to arsenic by oral gavage (0.38 mg/kg bd wt) for 30 days. On completion of the exposure, animals were sacrificed, and the level of myelin basic protein (MBP) was checked by immunofluorescence staining of the brain cryo-sections to investigate the status of myelin sheath in the same region of the brain ($+0.5$ mm to -1.5 mm in reference to bregma) of control and all the treatment groups. The level of MBP expression was almost half of the control in the cuprizone alone-exposed group, whereas the level of MBP expression was protected in cuprizone and arsenic co-exposed group. Arsenic alone-exposed group did not induce any significant alteration in MBP fluorescence compared to the control group (Fig. 2 A and B). The status of myelin sheath (corpus callosum) was also investigated by staining the corpus callosum of the same
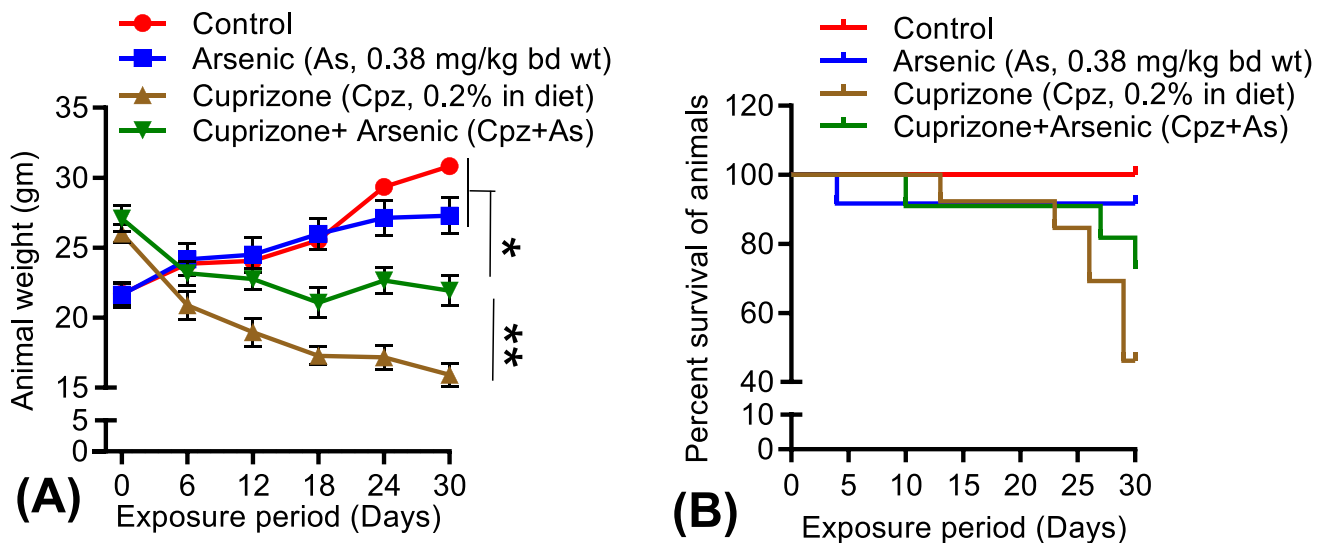
Fig. 1 Effect of arsenic and cuprizone exposure on body weight and survivability. Six to eight weeks old Balb/c mice were exposed to arsenic (sodium arsenite, 0.38 mg/kg bd wt) and cuprizone (0.2% in chow diet w/w) alone or in combination for 1 month. Arsenic was given through oral gavage, and cuprizone was mixed with a rodent chow diet (0.2% W/W). **A** Body weight of each mouse was recorded every week and represented as line graph. Values presented as mean ± SEM (standard error mean) of eight to nine animals. **B** Mice in control and treatment groups were monitored for 30 days for the survival analysis ($n = 11$). The day of death of each animal of every group was recorded and plotted as Kaplan–Meier survival curves showing the percent survivability of mice during the study. In both cases, arsenic co-treatment showed a protective effect against the cuprizone treatment. "n" denotes the number of animals used in the study. Each data point represents mean ± SEM. "p" denotes the level of significance in comparison to control; *$p < 0.05$; **$p < 0.01$; ***$p < 0.001$; ns, non-significant

region of the brain using a black-gold II myelin staining kit. A staining pattern similar to MBP was observed in black-gold II-stained brain sections. The arsenic-cuprizone co-exposed group showed protection against cuprizone-induced myelin sheath degeneration, whereas the arsenic-alone-exposed group was unaffected compared to the control group (Fig. 2 C and D). The status of myelin sheath wrapping around nerve axon was also investigated using transmission electron microscopy (TEM). The control animals showed tightly wrapped myelin sheath around the nerve axons; almost similar pattern was observed in the arsenic alone-exposed group. Following 30 days of cuprizone exposure, myelin sheath around the nerve axon was highly degenerated and showed exfoliating morphology. Interestingly, the ultrastructure of tightly wrapped myelin sheath was protected in the arsenic-cuprizone co-exposed group (Fig. 2E). From the TEM images, number of myelinated axons was counted, and the quantitative data generated was represented in a histogram (Fig. 2F). Therefore, it is evident from the data that arsenic protects cuprizone-induced demyelination of corpus callosum in Balb/c mice.

Microglial Inflammation Is Not Involved in the Arsenic-Mediated Protection of Demyelination of Corpus Callosum in Balb/c Mice

Microglial number increases in the corpus callosum during the demyelination and remyelination process, and microglial

neuroinflammation plays an important role in CPZ-induced demyelination. In the present study, we have measured the level of microglial IL-6/TNF-α in the culture supernatant of ex vivo microglia isolated from experimental animals. A higher level of cytokines was detected in arsenic alone exposure group; an even higher level of cytokine was detected in cuprizone-only exposure group. Interestingly, arsenic-cuprizone co-exposed group could not inhibit the cuprizone-induced increase in IL-6/TNF-α level (Fig. 3 A and B). The level of microglial activation marker, Iba1, was also checked through immunofluorescence staining of brain cryo-sections. An increased Iba1-associated fluorescence was observed in arsenic-alone exposed group, and an even higher fluorescence was detected in the cuprizone-alone exposed group. Interestingly, similar to cytokine, arsenic-cuprizone co-exposure could not reduce the microglial activation (Fig. 3 C and D). It seems that microglial neuroinflammation does not play any role in the protection of cuprizone-induced demyelination of corpus callosum by arsenic. Therefore, we co-exposed the experimental animals with cuprizone and minocycline, which is known to inhibit microglial inflammation. Black-gold II myelin-stained sections showed severe degeneration of myelin sheath in the corpus callosum of the cuprizone-exposed group, whereas almost no protection was observed in minocycline-cuprizone co-exposed group unlike that of arsenic-cuprizone co-exposed group (Fig. 3E). The level of microglial activation

(A)

(B)

(C)

(D)

Control — Intact corpus callosum (Myelin sheath)

Arsenic (As) — Intact corpus callosum (Myelin sheath)

Cuprizone (CPZ) — Damaged corpus callosum (Myelin sheath)

As+ CPZ — Protected corpus callosum (Myelin sheath)

(E)

(F)
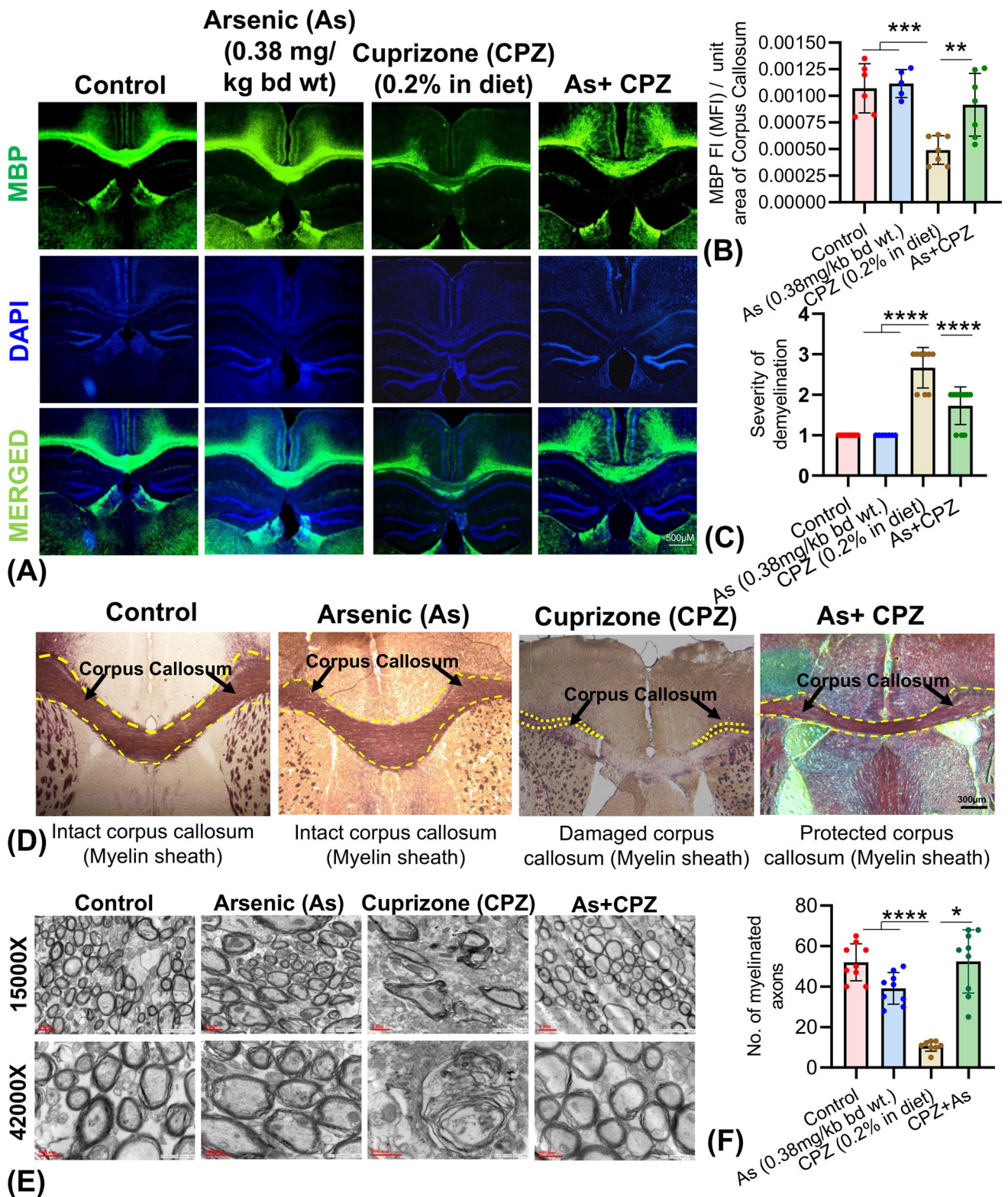
marker, Iba1, was also not decreased in minocycline-cuprizone co-exposed group (Fig. 3 F and G). Simultaneously, changes in the levels of cytokines were also measured in the ex vivo microglial culture supernatant. Similar to microglia activation marker, arsenic could not inhibit the cuprizone-induced increased level of IL-6 and TNF-α (Fig. 3 H and I). Interestingly, minocycline could inhibit the arsenic-induced microglial cytokine secretion (Fig. 3 J and K). Therefore,

◄**Fig. 2** Effect of arsenic on the cuprizone-induced demyelination of corpus callosum. Mice were exposed to arsenic and cuprizone alone or in combination for 1 month, as described earlier. Brains were isolated and processed for cryo-sectioning. Coronal brain sections were cut through the $+0.5$ mm to -1.5 mm from bregma. Brain sections were immunostained to check the myelin basic protein (MBP) immunoreactivity. **A** Representative images of MBP immunostained brain sections highlighting the corpus callosum region. Scale bar, 500 μm. **B** MBP-associated immunofluorescence was quantitated using "ImageJ" and represented as hybrid scatter-bar graph ($n = 5$–7 animals in each group). **C** Brain sections were also stained with black gold myelin stain to check the level of myelin sheath (corpus callosum) damage. Severity of the myelin sheath damage was measured from the Black gold myelin sheath stain-stained brain section through a double-blind fashion, and the severity of demyelination was rated on a three-point scale in which a higher, moderate, and lower score shows a lesser, medium, and greater pathology, respectively. The data were represented as hybrid scatter-bar graph ($n = 8$–9 animals in each group). **D** Representative images of Black gold myelin stain-stained sections showing the severity of myelin sheath damage. Scale bar, 300 μM. **E** Representative transmission electron micrographs showing the cross-section of myelinated axons in the corpus callosum. Severe damages in the myelin sheath were clearly visible in the cuprizone-exposed group, whereas protection of myelin sheath was observed in the cuprizone-arsenic co-exposed group. **F** Number of axons with intact myelin sheath was counted in each TEM images and presented as hybrid-bar graph ($n = 2$ animals in each group and one image from each of four to five sections from each animal were considered). Bar graph represents mean $\pm$ SD. p denotes the level of significance in comparison to control; *$p < 0.05$; **$p < 0.01$; ***$p < 0.001$; ns, non-significant

the data suggest that microglial neuroinflammation does not contribute to arsenic-mediated protection of cuprizone-induced demyelination of corpus callosum.

Arsenic Reverses the Cuprizone-Induced Impaired SOD Activity in Primary Oligodendrocytes and in Corpus Callosum Tissue of Balb/c Mice

Cuprizone impairs superoxide dismutase1 (SOD1) activity by chelating the free copper ions and thereby induces death of oligodendrocytes. In the present study, we have checked the viability of primary oligodendrocytes following in vitro exposure to cuprizone (400 μM) and arsenic (500 nM). Cuprizone exposure was observed to severely compromise the viability of primary oligodendrocytes ($\sim 55\%$ to control). Interestingly, the viability was protected in arsenic-cuprizone co-exposed primary oligodendrocytes. Arsenic-alone exposure did not affect the viability (Fig. 4A). In another experiment, $CuSO_4$ was supplemented as a source of copper ion, and as expected, it also protected the viability of primary oligodendrocytes similar to arsenic in cuprizone-$CuSO_4$ co-exposed group. $CuSO_4$ alone did not alter the viability (Fig. 4B). Furthermore, the SOD activity was investigated in these in vitro treatment groups. Cuprizone exposure was shown to severely compromise the SOD activity, whereas cuprizone-arsenic and cuprizone-$CuSO_4$

co-exposure protected the SOD activity. SOD activity in arsenic and $CuSO_4$ alone exposure group remained unaltered (Fig. 4C). Impaired SOD activity leads to increased reactive oxygen species (ROS) generation. Therefore, the level of cellular ROS was measured in primary oligodendrocytes following in vitro treatment using DCFDA. A significantly elevated level of ROS was observed only in the cuprizone-exposed group, whereas all other exposure groups showed insignificant alteration in cellular ROS level (Fig. 4D). Alteration in SOD activity in primary oligodendrocytes following in vitro exposure was validated in corpus callosum tissue of various exposure groups. A similar pattern of SOD activity was observed in corpus callosum tissue. The SOD activity was compromised in the cuprizone-exposed groups, whereas SOD activity was protected in the cuprizone-arsenic co-exposed group. SOD activity was unaltered in arsenic alone exposure group (Fig. 4E). It was observed that arsenic exposure does not affect the SOD activity both in vitro and in vivo. Therefore, molecular docking analysis was performed to check the possibility of binding of arsenic to SOD. The docking analysis revealed that arsenic cannot bind to SOD, and as expected, Cu can bind well with SOD (Fig. 4F).

Arsenic Competitively Binds to CPZ and Interferes in the Formation of Cu ↔ CPZ Complex

The findings of Messori et al. and Pushie et al. show the coordination chemistry of Cu ↔ CPZ complexation reaction wherein the copper can exist in two different oxidation states, Cu(II) and Cu(III) independently or simultaneously, based on the reactants stoichiometry and/or solvent effect [15, 26]. We also observed a similar trend in our mass analysis study for the structures of CPZ and CuCPZ. CPZ has the most abundant molecular ion peaks at m/z 139.09, 199.2, and 221.10, where the latter two peaks represent the monosodium adduct of mono hydrolyzed form (CPZmh) (Fig. 5A). A peak at m/z 301.16, the monosodium adduct of CPZ, is also observed in our case. For the CuCPZ complex, additional peaks at m/z 419.21 and m/z 501.10 were observed besides the above peaks (Fig. 5B, E). The other analyte peaks at m/z 457 and m/z 499.39 are consistent with the earlier reported data by Messori et al. Interestingly, the AsCPZ mass spectrum also has the observed dominant peaks of CPZ with a new peak at m/z 467.09 corresponding to bis-hydrolyzed cuprizone product of As ([As(CPZmh)$_2$]) (Fig. 5C, E). The fragment species formed in the case of Cu/AsCPZ co-complexation were the same as that of CuCPZ complex, with an additional new peak at m/z 467.09 of AsCPZ (Fig. 5D). The mass spectrum confirms the propensity of As(III) to form complex with CPZ in the presence of more dominant Cu(II) ions although in a subtle way.

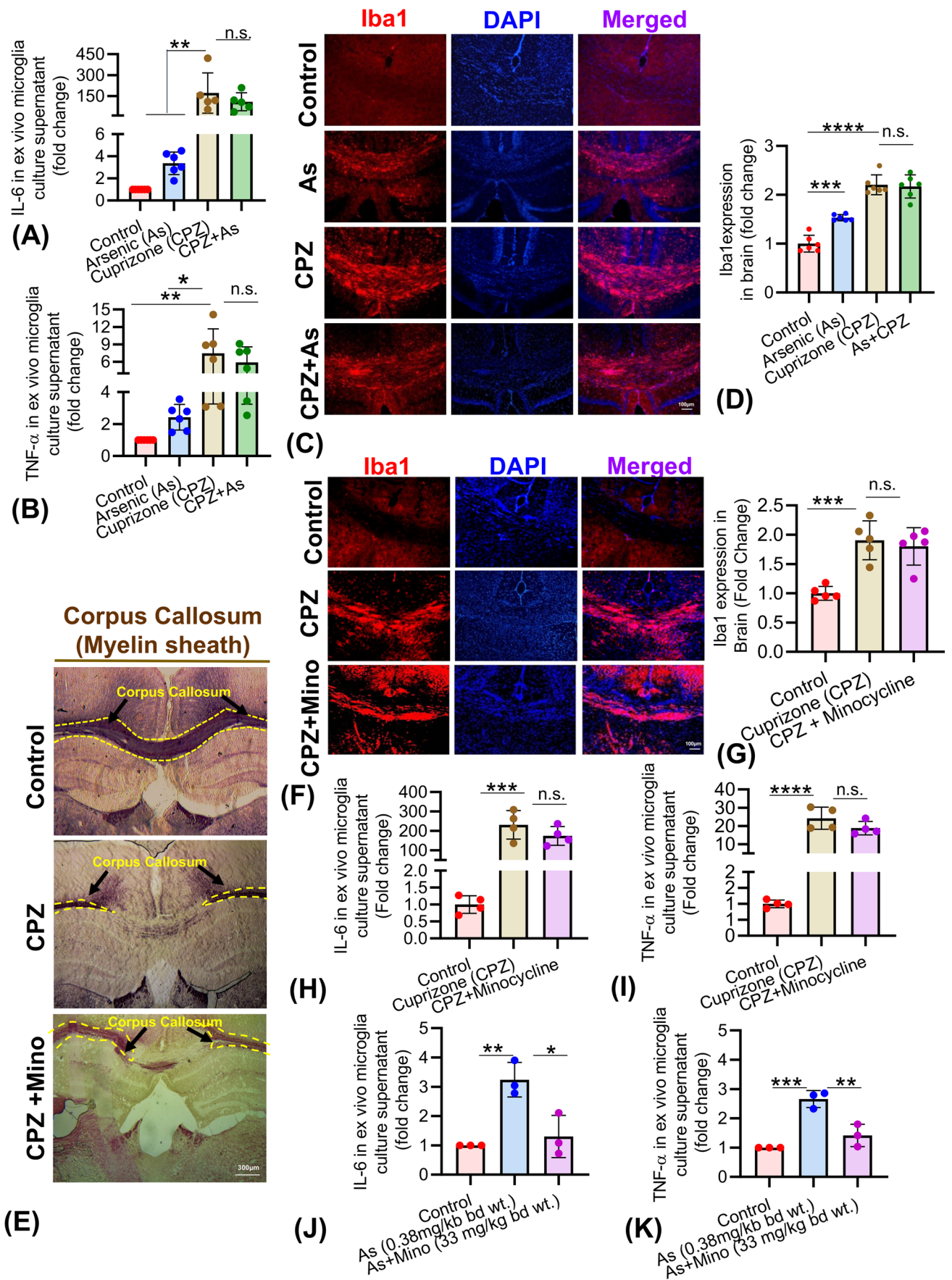Furthermore, the FTIR spectra revealed all the samples (CPZ, CuCPZ, AsCPZ, and Cu/AsCPZ) displayed prominent

◄**Fig. 3** Effect of microglial inflammation on cuprizone-induced demyelination of corpus callosum. Mice were exposed to arsenic and cuprizone alone or in combination for 1 month, as described earlier. Microglia were isolated from control and treated animals, cultured *ex vivo* for 18 h, and the level of cytokines was measured: **A** IL-6 and **B** TNF-α. The changes in the level of cytokines were expressed as fold changes in hybrid scatter-bar graph ($n = 5$–6 animals in each group). Another set of animals was also sacrificed; brains were isolated and processed for cryo-sectioning followed by immunostaining using microglial activation marker Iba1. **C** Representative images of Iba1-stained brain section highlighting the corpus callosum region. Scale bar, 100 µm. **D** Fold change of Iba1-associated immunofluorescence quantitated from the immunostained brain section using ImageJ and plotted as hybrid scatter-bar graph. In another experiment, animals were co-exposed to cuprizone and minocycline (33 mg/kg bd wt. through intra-peritoneal route). **E** Brains cryo-sections were stained with black gold myelin sheath stain to check the myelination status of corpus callosum. Scale bar, 300 µm. **F** Brain sections were also immune-stained with Iba1 antibody to check the activation status of microglia. Scale bar, 100 µm. **G** Fold change of Iba1-associated immunofluorescence quantitated from the immunostained brain section using ImageJ and plotted as hybrid scatter-bar graph. Primary microglia were isolated from another set of animals, cultured ex vivo for 18 h, and the level of cytokines measured in the culture medium. **H**, **I** IL-6/TNF-α in control, cuprizone, and cuprizone-minocycline co-exposed group. **J**, **K** IL-6/TNF-α in control, arsenic and arsenic-minocycline co-exposed group. Cytokine data were expressed as fold change in hybrid scatter-bar graph ($n = 3$–4 animals in each group). Bar graph represents mean ± SD. *p* denotes the level of significance in comparison to control; $*p < 0.05$; $**p < 0.01$; $***p < 0.001$; ns, non-significant

peaks in the region of 500–4000 cm^{-1} (Fig. 5F). The peaks at 3223 cm^{-1} correspond to the asymmetric stretching ($_{as}\nu$) N–H bond in aliphatic amine, while 2939 and 2862 cm^{-1} peaks highlight the C–H bond asymmetric stretching ($_{as}\nu$), and 1670 cm^{-1} peak corresponds to the characteristic C=O bond of CPZ (red curve). The above peaks of CPZ also appear in the CuCPZ (blue curve) and AsCPZ (pink curve) complexes, confirming the complexation reactions. Interestingly, the N–H bond in CPZ at 3223 cm^{-1} was observed to be shifted in CuCPZ and AsCPZ and appears at 653 cm^{-1} and 610 cm^{-1}, respectively, validating that the M↔CPZ complexation is occurring through CPZ$^{(2NN)}$ binding site (Fig. 5F; ball and stick figures). As expected, a similar pattern of spectral peaks along with fingerprint region is observed in the Cu/AsCPZ complex, again substantiating that As(III) can competitively bind to CPZ in the presence of Cu(II).

The ICP-MS analysis was performed to quantify the M(CPZ complexation reaction) (Fig. 5G). The amount of Cu (~ 1600 PPM) is substantially larger in the precipitate than that in the supernatant of CuCPZ complexation reaction, suggesting the strong affinity of Cu(II) to CPZ. Interestingly, in the co-complexation reaction (Cu/AsCpz) with the same reaction condition, the amount of copper is found to be less (~ 1300 PPM) when compared with CuCPZ reaction, substantiating that arsenic (10 PPM in precipitate) is

interfering in the CuCPZ complexation process. Moreover, the arsenic concentration in the supernatant of the AsCPZ and Cu/AsCPZ complexation was found to be significantly large (~ 1600 and 1700 ppm, respectively), suggesting a low degree of As↔CPZ complexation.

The DFT calculations revealed although the keto-imine binding MCPZ$^{(2NO)}$ (NO-coordinated trans-geometry) is theoretically the most stable structure, yet, it is surprising to find that the difference between the ground state energy of MCPZ$^{(2NN)}$ and MCPZ$^{(2NO)}$ is 3612 kJ/mol and 4974 kJ/mol for copper and arsenic complexes, respectively (Fig. 5H). Likewise, the energy difference between MCPZ$^{(2OO)}$ (OO-coordinated geometry) and MCPZ$^{(2NN)}$ is 1332 kJ/mole and 2978 kJ/mole for copper and arsenic complexes, respectively.

The energy profile diagram of all the possible reaction intermediates of As/Cu co-complexation reaction is shown in Fig. 5I. An activation energy of − 740 kJ mol^{-1} is required for the formation of CPZ transition state (TS-I) while the free energies of the formation of intermediate-I (CuCPZ interaction with As) and intermediate-II (AsCPZ interaction with Cu) were observed to be − 3725 kJ mol^{-1} and − 5651 kJ mol^{-1}, respectively. Copper ions were found to have a binding affinity with Pro-28 and Glu-21 at a distance of 2.97 Å and 3.0 Å, respectively, as shown in the close-up view. The lowest binding energy of Cu-SOD was calculated to be − 7.86 kcal mol^{-1} from the third docking. However, we could not find any observable interaction with SOD for arsenic ions.

Calorimetry directly measures the binding enthalpy under isobaric conditions ($q_p = \Delta H°$), allowing the binding entropy ($\Delta S°$) to be determined from the fundamental thermodynamic relationship ($\Delta G° = \Delta H° − T\Delta S°$) [37]. We observed that CuCPZ complexation had one exothermic binding event having a binding enthalpy (ΔH) of − 3697 ± 69.23 cal mol^{-1} and K_d value of 2.46E4 ± 2.01E3 M^{-1}. The stoichiometric number or the binding sites (n) was found to be 0.979 ± 0.0117 (Fig. 5J, K). However, the AsCPZ complexation has an enthalpy of − 5428 ± 249.0 and K_d value of 1.21E5 ± 2.73E4, with the predicted number of binding sites (n) found to be 0.329 ± 0.0111. The lower stoichiometry number (n) substantiates the thermodynamically unfavorable complex formation for As(III) with CPZ (Fig. 5K).

Arsenic Reverses Cuprizone-Induced Compromised Neurobehavior (Tail Suspension Test and Grip Strength Test)

Cuprizone-induced demyelinating mouse shows depressive behavior and motor deficits. To evaluate the impact of arsenic (0.38 mg/kg bd wt) on the cuprizone-induced (0.2% w/w in diet) depressive behavior, tail suspension test was performed following 30 days of exposure. A longer immobility time was observed in cuprizone-exposed animals
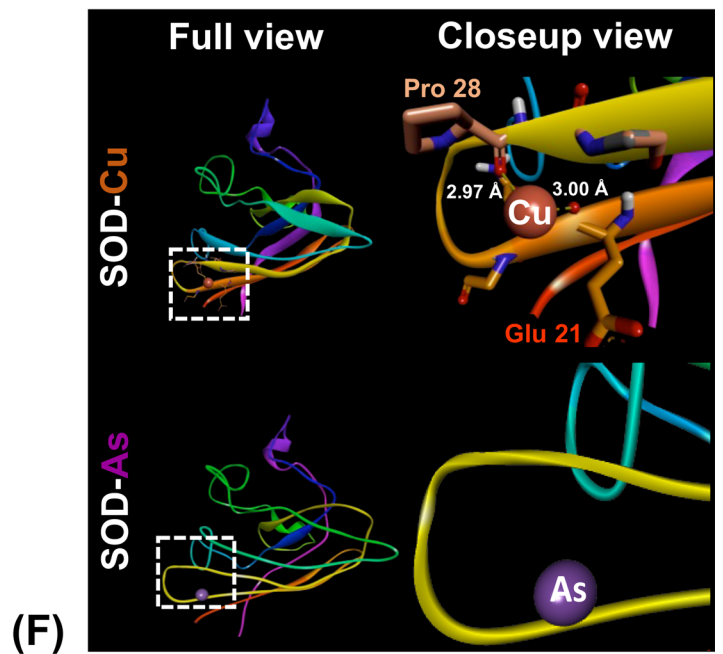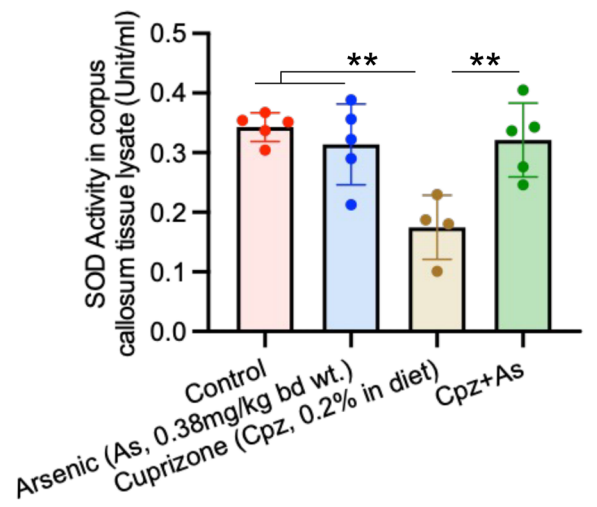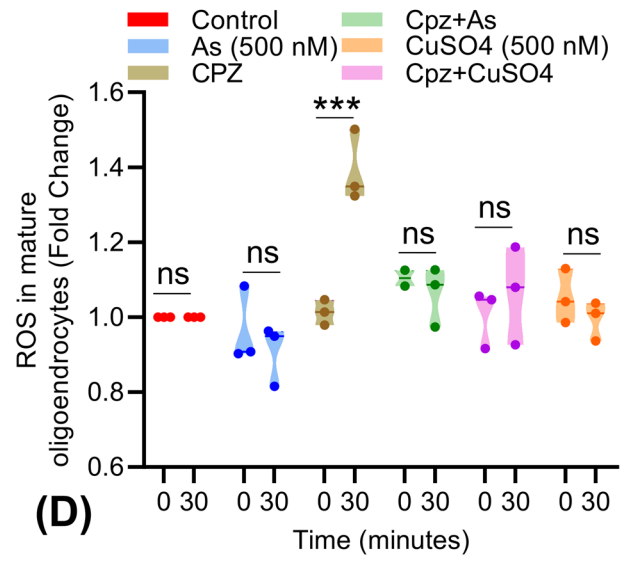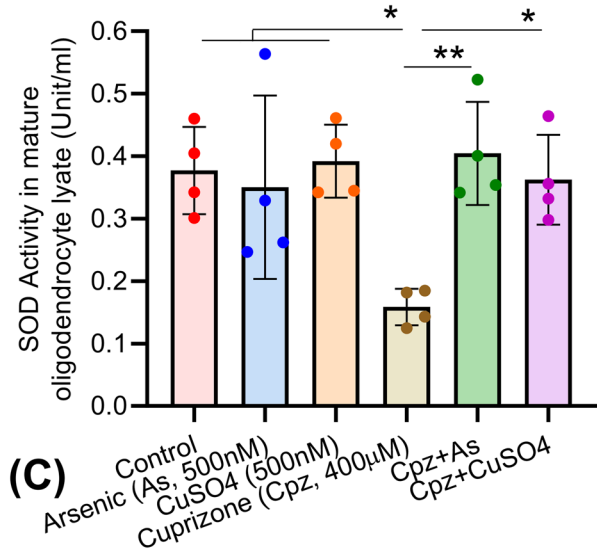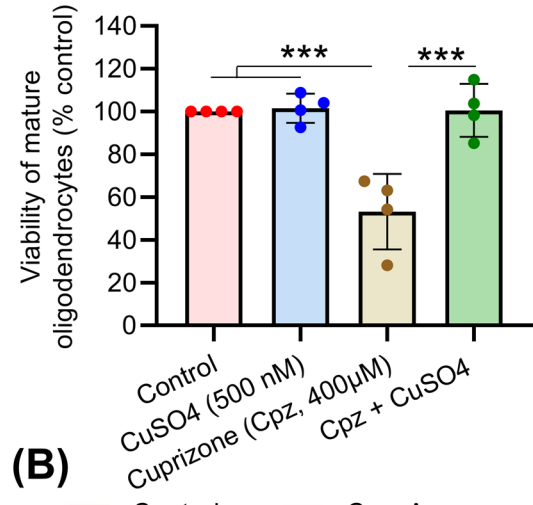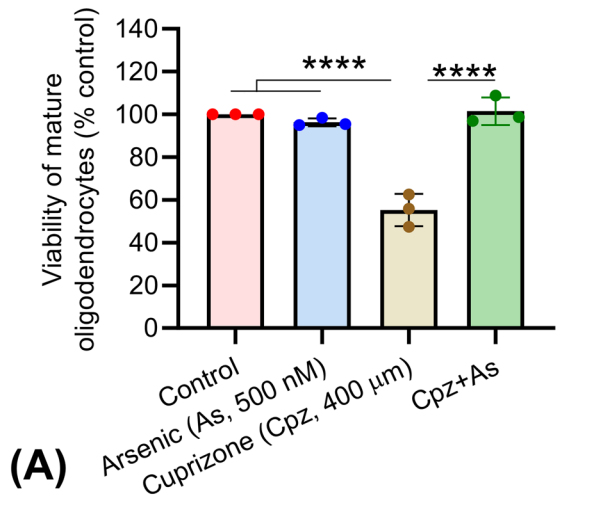
◀**Fig. 4** Effect of arsenic on the cuprizone-induced altered oligodendrocyte viability, SOD activity, and ROS production. Primary oligodendrocytes were differentiated from oligodendrocyte progenitor cells (OPCs) in cell culture plate. Mature oligodendrocytes were treated with cuprizone, arsenic, copper sulfate alone, and in combination for 24 and checked for the **A**, **B** viability, **C** super oxide dismutase (SOD) activity, and **D** reactive oxygen species (ROS) generation. $n = 3$–4 independent experiments. **E** SOD activity was also checked in the corpus callosum tissue of control and cuprizone/arsenic-treated animals. $n = 4$–5 animals in each group. **F** In silico analysis showed proper binding of copper to SOD, whereas no binding of arsenic to SOD was observed. Viability and SOD activity data were represented as hybrid scatter-bar graph, and the ROS data was represented as violin plots with individual data points. Bar graph represents mean $\pm$ SD. p denotes the level of significance in comparison to control; *$p < 0.05$; **$p < 0.01$; ***$p < 0.001$; ns, non-significant

compared to control animals, whereas the cuprizone-arsenic co-exposed animals showed a shorter immobility period compared to the cuprizone-exposed group. There was no difference in immobility time between the control and arsenic-only exposure group (Fig. 6A). To evaluate the impact of arsenic on the cuprizone-induced altered neuromuscular function, we performed grip strength test. The grip strength test is a non-invasive method designed to test neuromuscular function by determining the maximum force generated by experimental animals on pulling out of a specific grip. It was observed that 30 days of cuprizone exposure severely compromised the grip strength of the animals, whereas the cuprizone-arsenic co-exposed group showed better grip strength compared to the cuprizone-only exposure group. The arsenic-only exposure group did not have any significant impact on the grip strength of the experimental animals (Fig. 6B). To test grip strength, animals were given three trials. We have counted out of three trials how many times the test animal can hold the grip. It was observed that similar to the grip strength, cuprizone-arsenic co-exposed group showed better performance compared to cuprizone alone exposure group (Fig. 6C).

Discussion

The use of arsenicals against demyelinating diseases like multiple sclerosis has been tried for decades. Unfortunately, the trial led to the development of gastrointestinal and other side effects, possibly owing to the higher dose and long-term exposure regime of arsenic [38]. Interestingly, a study by Tsai and Lee reported a negative correlation between soil arsenic and the incidence of multiple sclerosis in Taiwan [39], which was supportive of our study. In the present study, we strongly prove that arsenic can inhibit oxidative stress by protecting the SOD1 activity in a CPZ-induced demyelinating mouse model and thereby protecting the myelin sheath. We performed in silico analysis, in vitro experiments with

primary oligodendrocytes, in vivo studies in Balb/c mice, and suitable neurobehavior tests further validated the results.

Weight loss and mortality are obvious outcomes in the CPZ-induced demyelinating mouse model [40], which were protected by the low dose of arsenic co-exposure, similar to flavonoid co-exposure [41]. Myelin basic protein (MBP), the major component of the myelin sheath, decreases in demyelinating diseases like MS and thereby affects the proper nerve impulse conduction. In the present study, CPZ exposure decreased the level of MBP as expected, whereas arsenic co-exposure protected the MBP expression as in the case of minocycline, baicalein, and ursolic acid [41–43] by inhibiting oxidative stress-related pathways. A similar pattern of protection of myelin sheath was observed in the corpus callosum region in the arsenic co-exposed group, as in the case of cannabidiol, ursolic acid, and curcumin [43–45]. TEM analysis of the corpus callosum tissue showed the protection of myelinated neurons in arsenic-exposed group, as earlier shown in exposure to cannabidiol or by over-expression of Sox10 in oligodendrocytes [45, 46]. Contrary to the protective effect of arsenic against the CPZ-induced demyelination in the present study, it was earlier shown to have a demyelinating effect. The toxic effect of arsenic may be due to the use of 30 times or 10 times higher doses of arsenic than the dose used in the present study, and arsenic-induced apoptosis was the reason for the demyelination [47, 48].

Neuroinflammation and oxidative stress play a pivotal role in inducing demyelination. The levels of neuroinflammatory markers were checked to deduce the mechanism of action. Studies with CPZ showed that microglial activation and proinflammatory cytokines like IL-6/TNF- α/ IL-1β are critical factors for oligodendrocyte death and demyelination [12], and their inhibition can protect the myelination status of corpus callosum [41, 42, 45]. In the present study, neither arsenic nor minocycline could inhibit the CPZ-induced microglial activation and inflammation significantly, maybe because the dose of minocycline used is not sufficient, although it could inhibit only arsenic-induced IL-6 and TNF-a where a lower level of inflammation was induced. Even though arsenic could not inhibit microglial activation and inflammation, it could protect the corpus callosum from CPZ-induced damage. Therefore, it is evident that arsenic-mediated protection of the corpus callosum is not channelized through the inflammatory pathway, thus making the involvement of the oxidative pathway evident in the event of arsenic-mediated protection of the corpus callosum.

Oxidative stress is a major contributor to the initiation and progression of demyelinating disease in the CNS [2–4]. Therefore, we studied the effect of arsenic co-exposure on the CPZ-induced viability of primary oligodendrocytes and oxidative stress. Arsenic co-exposure was observed to protect the viability of primary oligodendrocytes from the toxic effect of CPZ. A similar response was observed in the copper
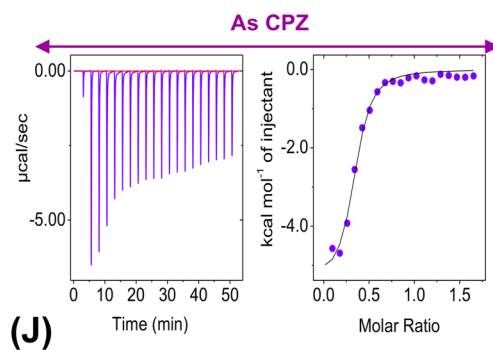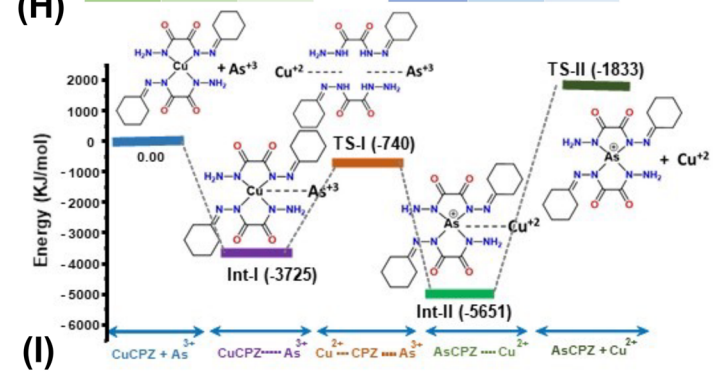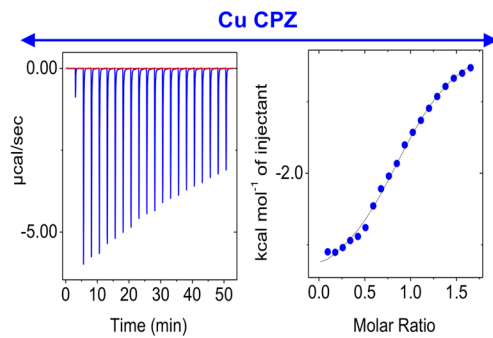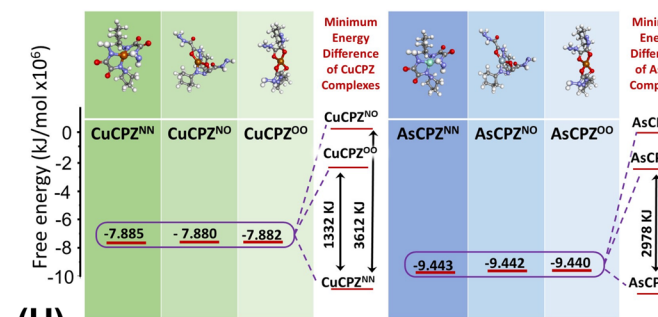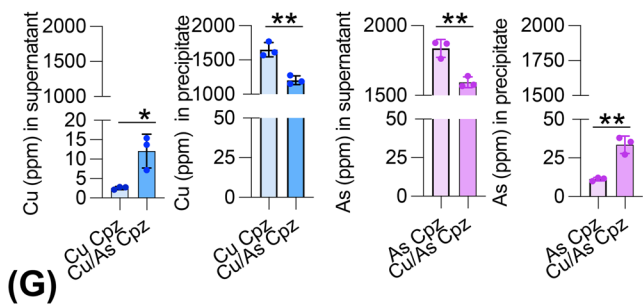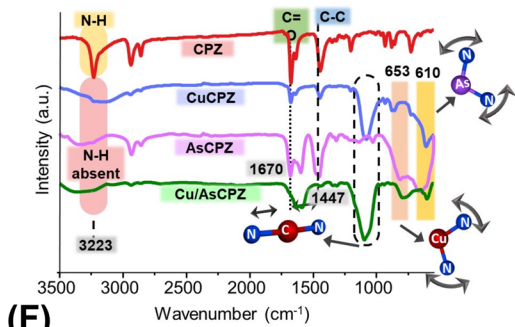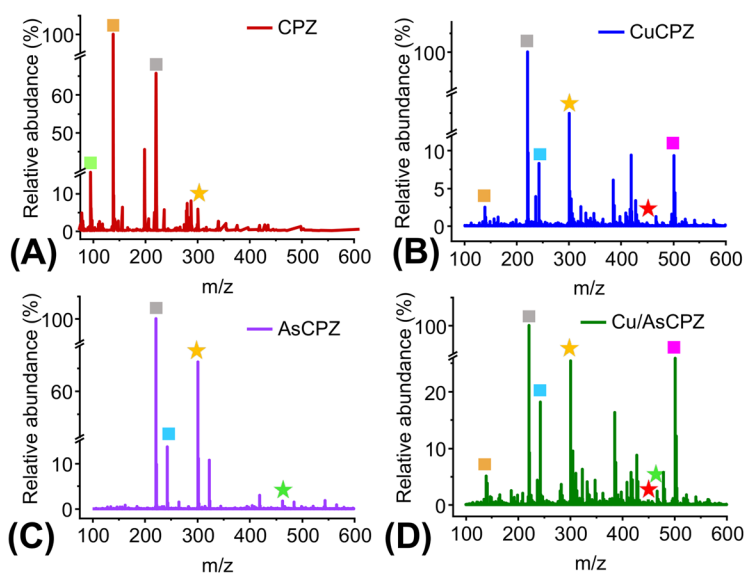
◀**Fig. 5** Binding of copper and arsenic to cuprizone. Mass spectra of M↔CPZ complexation reactions obtained in positive mode using direct injection ESI–MS. The spectra revealed various possible mass fragment patterns: **A** CPZ, **B** CuCPZ complex, **C** AsCPZ complex, and **D** Cu/AsCPZ complex showing fragments of both the precursor ion complexes. **E** Various possible mass fragments of CPZ and M↔CPZ complexes. **F** The highlighted overlay FTIR spectra of CPZ, CuCPZ, AsCPZ, and Cu/AsCPZ show the presence of CuCPZ binding peak (596 cm^{-1}) and AsCPZ binding peak (787 cm^{-1}) in the final Cu/AsCPZ complex confirming the formation of co-complex of both metal ions with CPZ. **G** ICP-MS analysis revealed that Cu effectively complexes with CPZ and gets precipitated, leaving a small amount of unreacted Cu in the supernatant as expected, while As binding to CPZ is significantly low, evident from a higher percentage of As still being present in the supernatant of AsCPZ complexation reaction. Interestingly, in the co-complexation reaction where both As and Cu ions are present, the data revealed the presence of As in the precipitate, suggesting As can competitively bind with CPZ in the presence of Cu, even though the latter has a higher preferential binding with CPZ.DFT energy profiling of possible geometries of cuprizone complex with copper and arsenic ions. Cu, As, CPZ, and their complexes' gas phase geometry were optimized to contain three different binding sites (NN, NO, OO). **H** DFT calculations were conducted at the B3LYP, 6-31G (for H) and 6-311G (d,p) as the basis set. **I** Relative ground-state energy profiling of M-CPZ^{NN} and their transition state geometry. **J** The ITC thermograph and integrated titration curve resulting from the binding reveal that the formation enthalpy of As↔CPZ complex is higher than that of Cu↔CPZ complex. **K** The thermodynamic parameters of the Cu and As ions binding to cuprizone at 310.15 K obtained from the ITC curves reveal both the complexation reactions to be exothermic in nature, yet the propensity of Cu to form a complex with CPZ is higher compared to As, evident from the higher number of stoichiometrically available binding sites vis-a-viz As

sulfate-supplemented group, indicating a possible inhibition of oxidative stress and consequent protection from apoptotic death of oligodendrocytes [5, 12]. SOD1 is one of the major antioxidative enzymes, and CPZ reduces the SOD1 activity by chelating copper ion [5] in oligodendrocytes, brain [49], hippocampus [50] or the corpus callosum [51]. We have also observed a similar result, an increased cellular ROS level, and impaired SOD activity in the CPZ-treated group, whereas no changes were observed in cellular ROS level and SOD activity in CPZ-arsenic co-exposed group compared to the control [6]. In support of the arsenic-mediated protection of SOD activity, we did in silico analysis and observed that arsenic cannot bind to the copper-binding site in SOD; therefore, apparently, arsenic does not affect the SOD function.

There is the possibility that arsenic can competitively bind to CPZ and, in turn, make the copper freely available in cytosol, which keeps up the SOD activity. To prove the binding of arsenic to CPZ, we did in silico analysis and performed experiments with analytical chemistry techniques. A spin-unrestricted DFT calculation was used to study the molecular and electronic structures of the CuCPZ and AsCPZ complexes. Three plausible chelation modes (MCPZ $^{(2NN)}$, MCPZ $^{(2NO)}$, and MCPZ $^{(2OO)}$) with different atomic centers were constructed with Cu^{2+} and As^{3+} cations and optimized by the Gaussian 16W software. DFT simulation studies reveal a few surprising outcomes: (a) although the keto-imine bond tautomerism MCPZ (2NO) is theoretically a more stable conformation compared to MCPZ (2NN), we
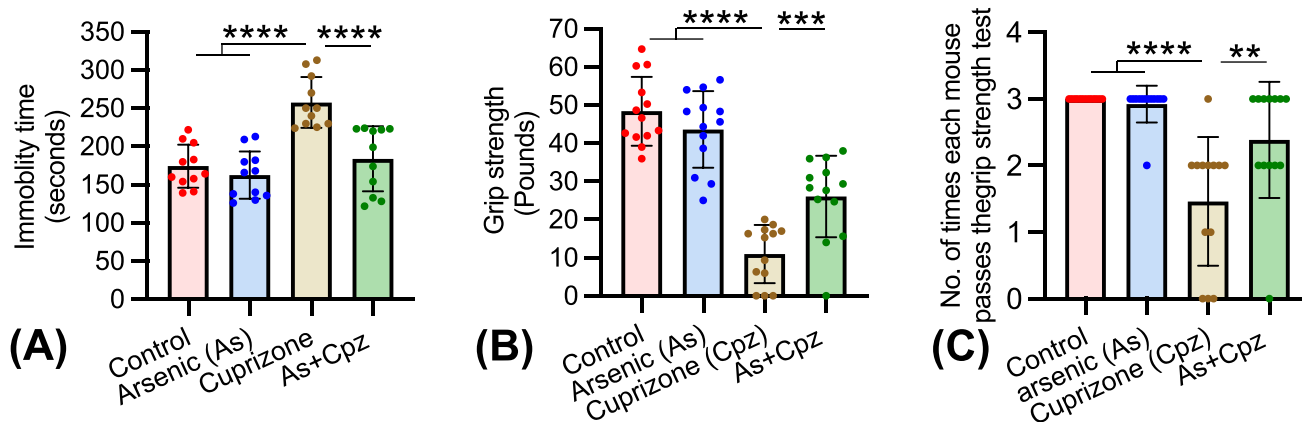

Fig. 6 Effect of arsenic on the depressive behavior and grip strength of cuprizone-exposed mice. Mice were exposed to arsenic and cuprizone, alone or in combination, for 1 month, as described earlier. Following 1 month of exposure, animals were subjected to neurobehavioral tests. **A** Tail suspension test records the immobilization time, which reflects the level of depression in animals. The immobilization times were recorded and expressed as hybrid scatter-bar graph. The test results showed an increased depressive behavior in cuprizone-exposed animals, whereas a protective effect was observed in arsenic-cuprizone co-exposed animals ($n=11$ animals in each group). **B, C**

Animals were also tested for neuro-motor function through a grip strength test. Strength of the grip was recorded in pounds for each animal and represented as hybrid scatter-bar graph. How many times the animal can hold the grip out of three trials was also recorded and represented as hybrid scatter-bar graph. In both cases, performance was compromised in cuprizone-expose group, whereas cuprizone-arsenic co-exposed group showed protection from the effect of cuprizone. Bar graph represents mean±SD. p denotes the level of significance in comparison to control; *$p<0.05$; **$p<0.01$; ***$p<0.001$; ns, non-significant

observed the latter had a lower ground state energy suggesting the possibility of CPZ binding with metal centers involving different binding sites than those with thermodynamically favorable conformations; (b) AsCPZ complexes have lower ground states irrespective of the site of coordination. These findings need to be looked upon in detail and beyond the scope of the present work. The energy profile diagram reveals that the first step was the rate-determining step of the complexation reaction. The apparent difference in activation energies of the CuCPZ–-As and AsCPZ–-Cu was observed around 1926 kJ mol^{-1} (0.733 Hartree), suggesting that As can competitively bind with CPZ in the presence of copper. Our mass analysis of the complexed products is in accordance with earlier-published literature [15, 26]. Interestingly, from the mass analysis, we found that As(III) can also form the AsCPZ complex, albeit with lesser propensity and can compete with more favorable copper ions for the CPZ binding sites when present together. The fact that As(III) can also form complexation with CPZ complex is reported here for the first time. The mass analysis was further supported by the FTIR analysis of the M $\leftrightarrow$ CPZ complexes. The ICP-MS analysis of all the complexed products in the individual and mixed metal reaction also corroborates the above findings. For the Cu/AsCPZ co-complex reaction, the amount of Cu present in the free form is around 12 PPM, while the bonded Cu(II) amount was around 1300 PPM. This difference in the individual and co-complexation reaction suggests As is indeed interfering in the CuCPZ complexation process by competitively seeking the CPZ ligand for complexation in the solution. Once it was established that the degree of complexation of both Cu(II) and As(III) with CPZ differed, the ITC experiments were performed to get insight into how thermodynamically these reactions are governed. Although the thermodynamic analysis reveals the difference in enthalpies of both the AsCPZ and CuCPZ complexation process to be exothermic, the number of available binding sites for the AsCPZ complex is found to be less ($n = 0.3$), suggesting a low probability of interaction between the two reacting species. However, the average binding sites for CuCPZ were found to be nearly 1 ($n = 0.98$), indicating a more thermodynamically favorable reaction. The above observations establish that arsenic in an in vivo scenario can competitively bind to CPZ and in doing so make some copper ions freely available for SOD activity, which in turn enables protection from CPZ-induced demyelination by arsenic.

With the mechanistic revelation of arsenic-mediated protection of demyelination, we wanted to validate our findings through neurobehavior tests. Demyelination is associated with improper neuronal function, which results in behavioral disorders like depression, anxiety, impaired cognition, and impaired motor function [52, 53]. In the present study, depressive behavior and motor function were tested using the tail suspension test and grip strength test. Depressive behavior was improved in arsenic-CPZ co-exposed group, as shown following venlafaxine and paenol treatment [54, 55]. Similar protection of motor function by arsenic was observed as reported with vit-D3, siponimod, and crocin treatment [56, 57]. Overall, the present study unraveled an interesting mechanism of arsenic-mediated protection of SOD1 activity and myelin status of corpus callosum in a CPZ-induced demyelinating mouse model.

Data Availability All data generated for this study are contained within the manuscript. For further queries, the corresponding author D. G. may be contacted.

Declarations

Ethics Approval All the protocols of the study were approved by the Institutional Animal Ethics Committee (IAEC) of the CSIR-IITR in Lucknow, India (IITR/IAEC/73/17). All experiments were conducted in accordance with the standards established by the CPCSEA of the Ministry of Environment and Forests, Government of India, New Delhi, India.

Consent to Participate No human data was used in the present work.

Consent for Publication No human data was used in the present work.

Competing Interests The authors declare no competing interests.

References

1. Love S (2006) Demyelinating diseases. J Clin Pathol 59(11):1151–1159
2. Gilgun-Sherki Y, Melamed E, Offen D (2004) The role of oxidative stress in the pathogenesis of multiple sclerosis: the need for effective antioxidant therapy. J Neurol 251:261–268

3. Tobore TO (2021) Oxidative/nitroxidative stress and multiple sclerosis. J Mol Neurosci 71(3):506–514

4. Nellessen A, Nyamoya S, Zendedel A, Slowik A, Wruck C, Beyer C, Fragoulis A, Clarner T (2020) Nrf2 deficiency increases oligodendrocyte loss, demyelination, neuroinflammation and axonal damage in an MS animal model. Metab Brain Dis 35:353–362

5. Vega-Riquer JM, Mendez-Victoriano G, Morales-Luckie RA, Gonzalez-Perez O (2019) Five decades of cuprizone, an updated model to replicate demyelinating diseases. Curr Neuropharmacol 17(2):129–141

6. Fukai T, Ushio-Fukai M (2011) Superoxide dismutases: role in redox signaling, vascular function, and diseases. Antioxid Redox Signal 15(6):1583–1606

7. Tvrdá E, Benko F (2020) Free radicals: what they are and what they do. In: Pathology. Elsevier, pp 3–13

8. Zhan J, Mann T, Joost S, Behrangi N, Frank M, Kipp M (2020) The cuprizone model: dos and do nots. Cells 9(4):843

9. Kipp M, Clarner T, Dang J, Copray S, Beyer C (2009) The cuprizone animal model: new insights into an old story. Acta Neuropathol 118:723–736

10. Matsushima GK, Morell P (2001) The neurotoxicant, cuprizone, as a model to study demyelination and remyelination in the central nervous system. Brain Pathol 11(1):107–116

11. Praet J, Guglielmetti C, Berneman Z, Van der Linden A, Ponsaerts P (2014) Cellular and molecular neuropathology of the cuprizone mouse model: clinical relevance for multiple sclerosis. Neurosci Biobehav Rev 47:485–505

12. Zirngibl M, Assinck P, Sizov A, Caprariello AV, Plemel JR (2022) Oligodendrocyte death and myelin loss in the cuprizone model: an updated overview of the intrinsic and extrinsic causes of cuprizone demyelination. Mol Neurodegener 17(1):1–28

13. Mason J, Jones J, Taniike M, Morell P, Suzuki K, Matsushima G (2000) Mature oligodendrocyte apoptosis precedes IGF-1 production and oligodendrocyte progenitor accumulation and differentiation during demyelination/remyelination. J Neurosci Res 61(3):251–262

14. Morell P, Barrett C, Mason J, Toews A, Hostettler J, Knapp G, Matsushima G (1998) Gene expression in brain during cuprizone-induced demyelination and remyelination. Mol Cell Neurosci 12(4–5):220–227

15. Messori L, Casini A, Gabbiani C, Sorace L, Muniz-Miranda M, Zatta P (2007) Unravelling the chemical nature of copper cuprizone. Dalton Trans 21:2112–2114. https://doi.org/10.1039/B701896G

16. Yamamoto N, Kuwata K (2009) DFT studies on redox properties of copper-chelating cuprizone: unusually high-valent copper (III) state. J Mol Struct (Theochem) 895(1–3):52–56

17. Venturini G (1973) Enzymic activities and sodium, potassium and copper concentrations in mouse brain and liver after cuprizone treatment in vivo. J Neurochem 21(5):1147–1151

18. Zagorski T, Dudek I, Berkan L, Mazurek M, Kedziora J, Chmielewski H (1991) Superoxide dismutase (SOD-1) activity in erythrocytes of patients with multiple sclerosis. Neurol Neurochir Pol 25(6):725–730

19. Ansari JA, Dey RK, Mishra SK, Roy O, Kushwaha S, Singh V, Patnaik S, Ghosh D (2022) Perinatal arsenic exposure-induced sustained microglial activation leads to impaired cognitive response in BALB/c mice. Neurotoxicology 92:1–14

20. Singh V, Kushwaha S, Ansari JA, Gangopadhyay S, Mishra SK, Dey RK, Giri AK, Patnaik S et al (2022) MicroRNA-129-5p-regulated microglial expression of the surface receptor CD200R1 controls neuroinflammation. J Biol Chem 298(1):101521

21. Singh V, Mitra S, Sharma AK, Gera R, Ghosh D (2014) Isolation and characterization of microglia from adult mouse brain: selected applications for ex vivo evaluation of immunotoxicological

22. alterations following in vivo xenobiotic exposure. Chem Res Toxicol 27(5):895–903

23. Chen Y, Balasubramaniyan V, Peng J, Hurlock EC, Tallquist M, Li J, Lu QR (2007) Isolation and culture of rat and mouse oligodendrocyte precursor cells. Nat Protoc 2(5):1044–1051

23. Sachs HH, Bercury KK, Popescu DC, Narayanan SP, Macklin WB (2014) A new model of cuprizone-mediated demyelination/remyelination. ASN Neuro 6 (5) https://doi.org/10.1177/1759091414551955

24. Chatterjee M, Jaiswal M, Palit G (2012) Comparative evaluation of forced swim test and tail suspension test as models of negative symptom of schizophrenia in rodents. Int Sch Res Not 2012

25. Terry AV, Gearhart DA, Beck WD, Truan JN, Middlemore M-L, Williamson LN, Bartlett MG, Prendergast MA et al (2007) Chronic, intermittent exposure to chlorpyrifos in rats: protracted effects on axonal transport, neurotrophin receptors, cholinergic markers, and information processing. J Pharmacol Exp Ther 322(3):1117–1128

26. Pushie MJ, Summers KL, Nienaber KH, Pickering IJ, George GN (2022) Synthesis and structural characterization of copper–cuprizone complexes. Dalton Trans 51(27):10361–10376. https://doi.org/10.1039/D2DT01475K

27. Taraboletti A, Walker T, Avila R, Huang H, Caporoso J, Manandhar E, Leeper TC, Modarelli DA et al (2017) Cuprizone intoxication induces cell intrinsic alterations in oligodendrocyte metabolism independent of copper chelation. Biochemistry 56(10):1518–1528. https://doi.org/10.1021/acs.biochem.6b01072

28. Huey R, Morris GM, Forli S (2012) Using AutoDock 4 and AutoDock vina with AutoDockTools: a tutorial. Scripps Res Inst Mol Graph Lab 10550:92037

29. Song C, Tian Z, Wang C, Shi R, Liu J (2021) Growth behavior and properties of (HF) 1–16 clusters. Struct Chem 32(1):395–403

30. Favila A, Gallo M, Glossman-Mitnik D (2007) CHIH-DFT determination of the molecular structure infrared spectra, UV spectra and chemical reactivity of three antitubercular compounds: rifampicin, Isoniazid and Pyrazinamide. J Mol Model 13(4):505–518

31. Berman HM, Battistuz T, Bhat TN, Bluhm WF, Bourne PE, Burkhardt K, Feng Z, Gilliland GL et al (2002) The protein data bank. Acta Crystallogr D Biol Crystallogr 58(6):899–907

32. Jafri H, Khan MSA, Ahmad I (2019) In vitro efficacy of eugenol in inhibiting single and mixed-biofilms of drug-resistant strains of Candida albicans and Streptococcus mutans. Phytomedicine 54:206–213

33. Kundu S, Mondal A, Weyhermüller T, Sproules S, Ghosh P (2016) Molecular and electronic structures of copper-cuprizone and analogues. Inorg Chim Acta 451:23–30

34. Bauernschmitt R, Ahlrichs R (1996) Treatment of electronic excitations within the adiabatic approximation of time dependent density functional theory. Chem Phys Lett 256(4–5):454–464

35. Miehlich B, Savin A, Stoll H, Preuss H (1989) Results obtained with the correlation energy density functionals of Becke and Lee, Yang and Parr. Chem Phys Lett 157(3):200–206

36. Rassolov VA, Pople JA, Ratner MA, Windus TL (1998) 6–31G* basis set for atoms K through Zn. J Chem Phys 109(4):1223–1229

37. Brautigam CA, Zhao H, Vargas C, Keller S, Schuck P (2016) Integration and global analysis of isothermal titration calorimetry data for studying macromolecular interactions. Nat Protoc 11(5):882–894. https://doi.org/10.1038/nprot.2016.044

38. Robertson D, Low-Beer T (1983) Long term consequences of arsenical treatment for multiple sclerosis. Br Med J (Clin Res Ed) 286(6365):605

39. Tsai CP, Lee CT (2013) Multiple sclerosis incidence associated with the soil lead and arsenic concentrations in Taiwan. PLoS One 8(6):e65911. https://doi.org/10.1371/journal.pone.0065911

40. Zhen W, Liu A, Lu J, Zhang W, Tattersall D, Wang J (2017) An alternative cuprizone-induced demyelination and remyelination mouse model. ASN Neuro 9(4):1759091417725174

41. Hashimoto M, Yamamoto S, Iwasa K, Yamashina K, Ishikawa M, Maruyama K, Bosetti F, Yoshikawa K (2017) The flavonoid Baicalein attenuates cuprizone-induced demyelination via suppression of neuroinflammation. Brain Res Bull 135:47–52

42. Pasquini LA, Calatayud CA, Bertone Una A, Millet V, Pasquini JM, Soto EF (2007) The neurotoxic effect of cuprizone on oligodendrocytes depends on the presence of pro-inflammatory cytokines secreted by microglia. Neurochem Res 32:279–292

43. Honarvar F, Hojati V, Bakhtiari N, Vaezi G, Javan M (2019) Myelin protection by ursolic acid in cuprizone-induced demyelination in mice. Iran J Pharm Res IJPR 18(4):1978

44. ELBini-Dhouib I, Manai M, Neili N-e, Marzouki S, Sahraoui G, Ben Achour W, Zouaghi S, BenAhmed M et al (2022) Dual mechanism of action of curcumin in experimental models of multiple sclerosis. Int J Mol Sci 23(15):8658

45. Sajjadian M, Kashani IR, Pasbakhsh P, Hassani M, Omidi A, Takzare N, Clarner T, Beyer C et al (2017) Protective effects of cannabidiol on cuprizone-induced demyelination in C57BL/6 mice. J Contemp Med Sci 3(11):278–283

46. Shao Y, Ding J, He QX, Ma QR, Liu Q, Zhang C, Lv HW, Liu J (2020) Effect of Sox10 on remyelination of the hippocampus in cuprizone-induced demyelinated mice. Brain Behav 10(6):e01623. https://doi.org/10.1002/brb3.1623

47. Rai NK, Ashok A, Rai A, Tripathi S, Nagar GK, Mitra K, Bandyopadhyay S (2013) Exposure to As, Cd and Pb-mixture impairs myelin and axon development in rat brain, optic nerve and retina. Toxicol Appl Pharmacol 273(2):242–258

48. Niño SA, Chi-Ahumada E, Ortíz J, Zarazua S, Concha L, Jiménez-Capdeville ME (2020) Demyelination associated with chronic arsenic exposure in Wistar rats. Toxicol Appl Pharmacol 393:114955

49. Fries M, Mertens M, Teske N, Kipp M, Beyer C, Willms T, Valkonen A, Rissanen K et al (2019) Water-soluble cuprizone derivative: synthesis, characterization, and in vitro studies. ACS Omega 4(1):1685–1689

50. Omotoso G, Olajide O, Gbadamosi I, Adebayo J, Enaibe B, Akinola O, Owoyele B (2019) Cuprizone toxicity and Garcinia kola biflavonoid complex activity on hippocampal morphology and neurobehaviour. Heliyon 5(7):e02102

51. Kashani IR, Chavoshi H, Pasbakhsh P, Hassani M, Omidi A, Mahmoudi R, Beyer C, Zendedel A (2017) Protective effects of erythropoietin against cuprizone-induced oxidative stress and demyelination in the mouse corpus callosum. Iran J Basic Med Sci 20(8):886

52. Sriramoju B, Kanwar RK, Kanwar JR (2015) Neurobehavioral burden of multiple sclerosis with nanotheranostics. Neuropsychiatr Dis Treat 2675–2689

53. Wajda DA, Sosnoff JJ (2015) Cognitive-motor interference in multiple sclerosis: a systematic review of evidence, correlates, and consequences. BioMed Res Int 2015

54. Pourmohammadi S, Kiasalari Z, Khalili M, Roghani M (2021) The effect of paeonol on motor deficits and depressive and anxiety-like behavior in cuprizone-induced model of multiple sclerosis. J Basic Clin Pathophysiol 9(2):49–54

55. Zhang Y, Bi X, Adebiyi O, Wang J, Mooshekhian A, Cohen J, Wei Z, Wang F et al (2019) Venlafaxine improves the cognitive impairment and depression-like behaviors in a cuprizone mouse model by alleviating demyelination and neuroinflammation in the brain. Front Pharmacol 10:332

56. Al-Otaibi KM, Alghamdi BS, Al-Ghamdi MA, Mansouri RA, Ashraf GM, Omar UM (2023) Therapeutic effect of combination vitamin D3 and siponimod on remyelination and modulate microglia activation in cuprizone mouse model of multiple sclerosis. Front Behav Neurosci 16:498

57. Tashakori A, Hassanpour S, Vazir B (2023) Protective effect of crocin on cuprizone-induced model of multiple sclerosis in mice. Naunyn-Schmiedeberg's Arch Pharmacol 1–13